HOST UNIVERSITY: The University of Edinburgh – The University of Queensland

FACULTY: School of Engineering – The Faculty of Engineering, Architecture and Information Technology

DEPARTMENT: Institute of Infrastructure and Environment – School of Civil Engineering

Academic Year 2016-2017

OPTIMISED FIRE SAFE AND ENERGY EFFICIENT DESIGN OF INSULATED ASSEMBLIES USING A MULTI-CRITERIA APPROACH

Pascale Vacca

Promoters:

Dr Juan P. Hidalgo

Dr Stephen Welch

Master thesis submitted in the Erasmus+ Study Programme

International Master of Science in Fire Safety Engineering

Abstract

The need to reduce energy consumption in buildings has led to increased use of insulation materials. Some insulation materials are combustible, which introduce a fire hazard since the pyrolysis onset may be achieved quickly, thus reducing the available safe egress time.

The objective of this thesis is to establish a framework to design assemblies consisting of insulation based on a multi-criteria approach, accounting for fire safety and energy efficiency. Quantitative performance-based methodologies are presented for both principles. Numerical analyses are performed to determine the performance of assemblies consisting of insulation (PIR, EPS and PF) and lining (MgO, plasterboard and brick) of different thickness. Results are compared to established critical performance criteria used to define failure (critical time and critical heat loss). Through both models optimum thicknesses are identified.

Non-combustible insulation assemblies (deemed fire safe) are further considered. Assuming the established acceptable fire performance, combustible solutions show a thickness approximately 10% thinner than non-combustible solutions for optimal energy efficiency performance. Metal-faced combustible insulation assemblies, also investigated, however always show prompt failure from a fire safety perspective.

In order to validate the fire methodology, numerical and experimental data are compared. Results indicate that, due to founding assumptions, this methodology is conservative.

Riassunto

Il bisogno di ridurre il consumo energetico negli edifici ha portato ad un aumento dell'utilizzo di materiali isolanti. Alcuni di questi materiali sono però combustibili, e creano quindi un pericolo d'incendio, dato che il principio di pirolisi può avvenire velocemente, riducendo il tempo a disposizione per un'evacuazione sicura.

L'obiettivo di questa tesi è quello di stabilire un quadro di riferimento per la progettazione di sistemi costruttivi che contengono materiali isolanti basato su un approccio con molteplici criteri, tenendo conto dei principi di sicurezza antincendio ed efficienza energetica.

Per entrambi i principi, vengono presentate metodologie quantitative basate sulla prestazione. Analisi numeriche sono effettuate per determinare la prestazione di sistemi costruttivi che contengono materiali isolanti (PIR, EPS e PF) e rivestimenti (MgO, cartongesso e mattoni) di diversi spessori. I risultati ottenuti sono confrontati per stabilire i criteri di prestazione critici utilizzati per definire un'insufficienza per quanto riguarda il tempo critico e le perdite di calore critiche. Tramite entrambi i modelli può essere identificato uno spessore ottimale.

Vengono inoltre considerati sistemi costruttivi con materiali isolanti non combustibili, ritenuti sicuri dal punto di vista della sicurezza antincendio. Supponendo che i sistemi costruttivi contenenti materiali combustibili siano sicuri da questo punto di vista, questi dimostrano di essere più sottili di circa il 10% rispetto a soluzioni non combustibili per quanto concerne l'efficienza energetica. Vengono studiati anche sistemi costruttivi con rivestimenti in metallo e materiali isolanti combustibili, che però si mostrano sempre insufficienti dal punto di vista della sicurezza antincendio.

Per poter convalidare la metodologia utilizzata per quanto riguarda il fuoco, sono messi a confronto dati numerici e sperimentali. A causa delle supposizioni fatte per entrambe le metodologie, i risultati ottenuti indicano valori più prudenti rispetto alla realtà.

Contents

List of Figures

List of Tables

1 Introduction and Objectives

1.1 Background

Energy consumption in buildings adds up to about 40% of the global energy use, and the building sector is the largest contributor to global Greenhouse gas emissions [1]. Heating and cooling are the main energy consumers in this sector, accounting for two thirds of a building's total energy consumption [2].

This has become a worldwide problem, and many countries are adopting sustainable design methodologies for the built environment in order to reduce their high energy consumption values.

Within the European Union, Member States are obliged to implement requirements for all new buildings to be Nearly Zero Energy Buildings by the end of the year 2020 [3]. Also, by the start of the year 2019, Member States must ensure that all new buildings occupied and owned by public authorities are Nearly Zero Energy Buildings as well [4]. A Nearly Zero Energy Building is a building with a very high energy performance, meaning that the building's energy requirement is nearly zero or very low [4].

According to the Directive 2010/31/EU of the European Parliament and of the Council of 19 May 2010, Member States must set minimum requirements for the energy performance of buildings and building elements which should achieve a cost-optimal balance between the investments and the costs saved through the lifecycle of the building.

Member States have to apply a methodology for the calculation of the energy performance which should take into consideration, among many other aspects, the thermal characteristics of the building. The Directive, however, does not specify one approach that all Member States should follow, but simply provides guidelines, giving the opportunity for each State to develop its own methodology. Currently there is a large variation in the way minimum energy performance requirements are specified and calculated: existing requirements vary between kWh/m² per year, relative CO_2 emission reduction, and different types of energy performance coefficients or indicators [3].

One of these energy performance indicators is the thermal transmittance, or U-value [W/m²K], which is the rate of transfer of heat through a structure, divided by the difference in temperature across that structure [5], along with its reciprocal, the R-value, or thermal resistance [m^2K/W]. Highly insulated structures achieve lower U-values [5], implying that insulation materials are inevitably required to achieve buildings with enhanced energy performance. However, this statement is only true when a steady-state condition is considered, because this assumption is only valid when daily and monthly temperature fluctuations remain within a narrow range.

1.2 Identification of the problem

The need to reduce energy consumption in buildings has led to an increased use of assemblies which include insulation materials in the building and construction industry. These materials help to effectively reduce heat losses from conditioned habitable spaces within the building to

the outside, as well as heat gains from the outside to these spaces. Also, the energy saved during the lifetime of these materials is more than the energy used for their production [6]. Figure 1 shows that the main types of thermal insulation materials utilized in the European market correspond to inert materials such as glass or stone wool, and plastic materials such as expanded and extruded polystyrene (EPS/XPS), phenolic foams (PF), and urethane/isocyanate-based foams (PUR/PIR).

Figure 1: European Thermal Insulation Market [7]

Glass and stone wool are inorganic, non-combustible, fibrous materials [8]. In contrast, the other main type of insulation materials used in construction are commonly made of rigid plastic foams [9], which are combustible and thus represent a hazard when it comes to fire safety in the built environment.

Combustible insulation materials are more energy efficient compared to non-combustible materials, as they offer a superior thermal performance [10]. However, they create several risks when it comes to fire safety.

Figure 2 gives examples of glass and stone wool. Glass wool is made from fibreglass, while stone wool is made from molten rocks (lava).
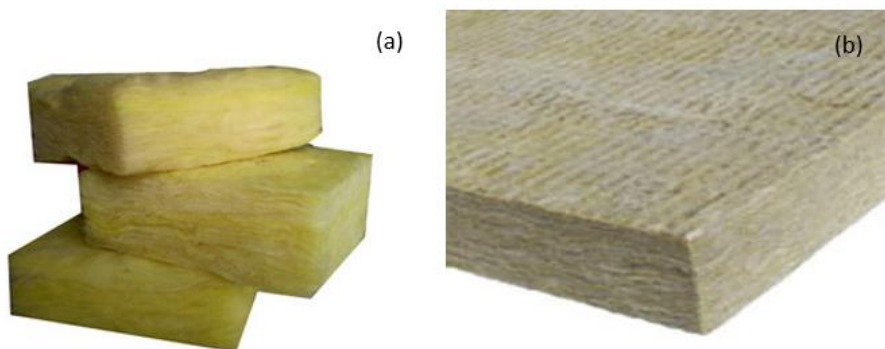
Figure 2: Example of (a) glass wool and (b) stone wool [11] [12]

Figure 3 shown an example of EPS and XPS. Both materials show melting and shrinking behaviours when exposed to high temperatures.
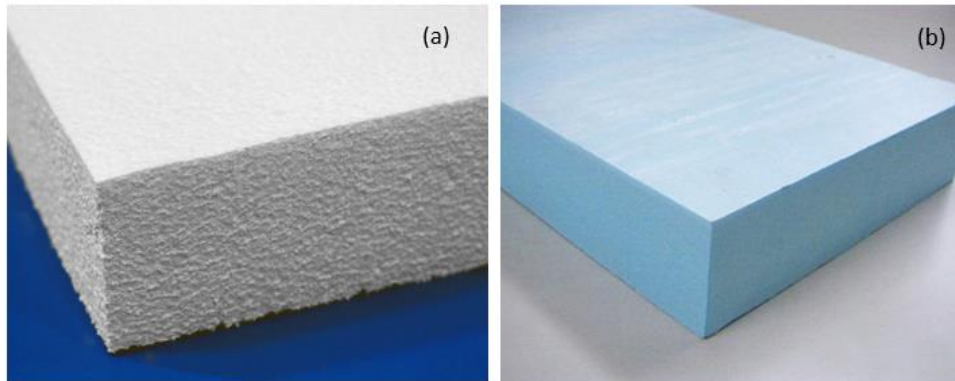
Figure 3: Example of (a) EPS and (b) XPS [13] [14]

Phenolic foam, as well as PIR and PUR, present charring when exposed to heat fluxes with values above their critical heat flux. Examples of these materials are shown in Figure 4 and Figure 5.

Figure 4: Example of phenolic foam [15]
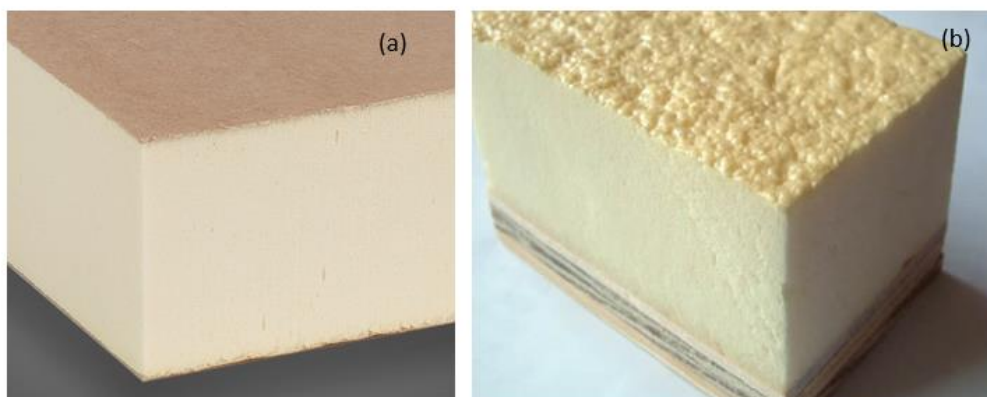
Figure 5: Example of (a) PIR and (b) PUR [16] [17]

Insulation materials are characterised by a low density (ρ) and an extremely low thermal conductivity (k) [18]. The product of these two material properties, along with the specific heat capacity (c), gives the thermal inertia ($k\rho c$) [19], which represents the ability of a material to conduct heat into its surface and to store this heat behind the surface [20]. Insulation materials are thus characterised by a low thermal inertia, which leads to rapid ignition and flame spread across the surface of the material [21]. Therefore, modest amounts of energy are required to achieve the onset of pyrolysis at the surface [22], where the temperature rises quickly [23], and maximum rates of burning are achieved in a short period of time [21].

When combustible insulation materials with a low thermal inertia are directly exposed to a fire, their fast ignition and flame spread is the main hazard from a fire safety perspective; this because untenable conditions in the compartment will be reached faster due to the quicker contribution to the heat release rate of the fire, impacting the available safe egress time.

When insulation materials are encapsulated, the hazard created by the onset of pyrolysis is delayed, but not avoided. Once pyrolysis occurs, a subsequent hazard is generated by the release of the flammable gases into the compartment affected by the fire, or elsewhere in the building. If these gases are released where the fire source is located, they will ignite, thus contributing to the heat release rate; if they are transported elsewhere, the hazard consists in their ability to ignite, thus allowing for fire spread, as well as in their intrinsic toxicity, which could impact evacuation.

1.2.1 Construction systems

Novel sustainable construction assemblies which encapsulate these combustible insulation materials are [24]:

- Structurally Insulated Panel systems (SIPs);
- metal faced insulated sandwich panels;
- External Thermal Insulation Construction (ETICs).

All these construction types are relatively cost effective and low weight compared to other traditional construction methods [24]. Also timber framed systems and masonry walls can include insulation materials. These construction systems are quite traditional, but still evolving to adapt to fit the new energy performance criteria.

Structurally Insulated Panel systems (SIPs) are used for residential and light commercial constructions. They consist of an insulating foam core (i.e. EPS, XPS, PIR, mineral wool etc. [25]) positioned between two structural linings, as shown in Figure 6 [26].

Figure 6: SIP system [27]

Metal faced sandwich panels are made out of a rigid polyurethane foam core which joins the metal panels together, which are made out of either surface-treated aluminium, steel sheets, or glass fibre-reinforced plastic laminates [28], as shown in Figure 7.
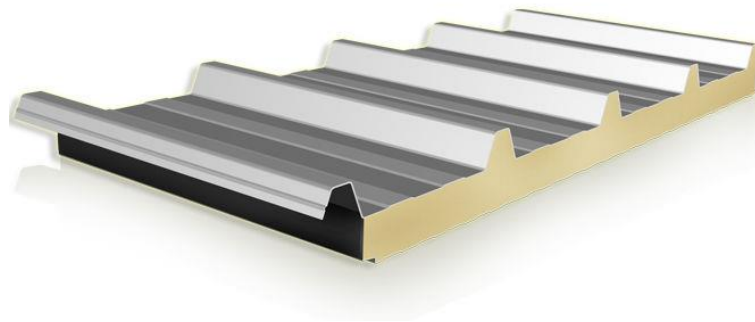
Figure 7: Metal faced sandwich panel [25]

External Thermal Insulation Composite systems (ETICs) contain an insulation material, such as EPS or mineral wool [29], a layer of adhesive, mechanical fixings, a reinforced layer, and the top coat finish, which is weatherproof [30], as can be seen in Figure 8. These systems are attached to external masonry walls.
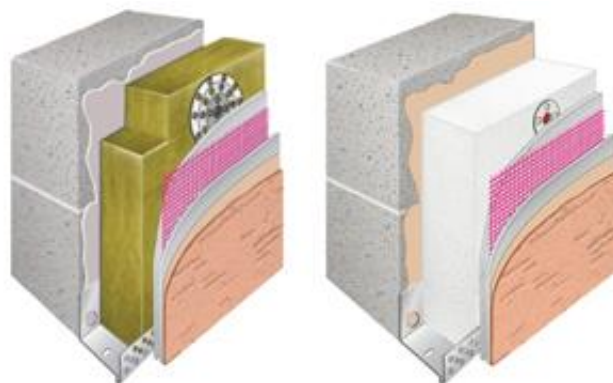
Figure 8: Examples of ETICs [31]

5

As shown in Figure 9, timber framed systems are based on the use of studs which create frames for the walls of the compartment. These studs produce a gap where the insulation is fitted, which will then be covered by a sheathing board on the outer face and plasterboard on the inner face. The insulation materials commonly used are PIR, EPS, PUR, PF, stone wool and glass wool [8].
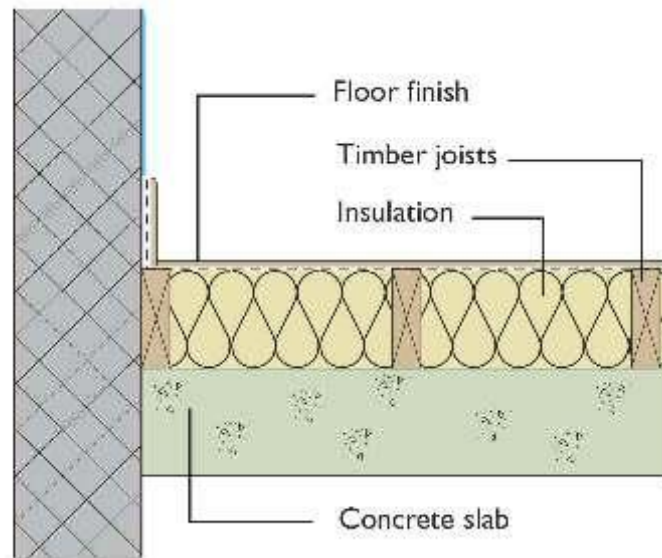
Figure 9: Example of a timber framed system [32]

An example of masonry walls which include insulation materials is given in Figure 10. Insulation materials utilized to fill the cavity of the wall include EPS, PIR, stone wool, and glass wool [8].
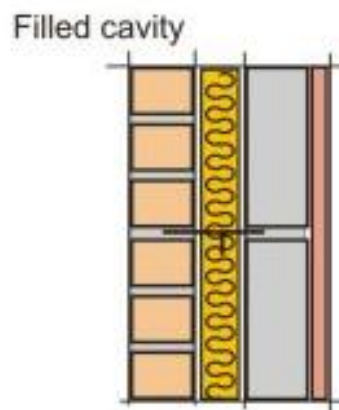
Figure 10: Example of filled masonry walls [33]

1.2.2 Principles for a fire safe design

When it comes to the design of fire safety strategies in buildings, two different stages of a compartment fire are classically considered: the pre-flashover and the post-flashover fire. Figure 11 shows the evolution of a fire in terms of heat release rate. The pre-flashover stage corresponds to a well-ventilated (fuel-controlled) fire, deemed less severe, characterised by lower temperatures and heat fluxes. The post-flashover stage corresponds to a ventilation

controlled fire, deemed more severe, characterised by high gas-phase temperatures, burning rates and heat fluxes to the boundaries of the compartment.
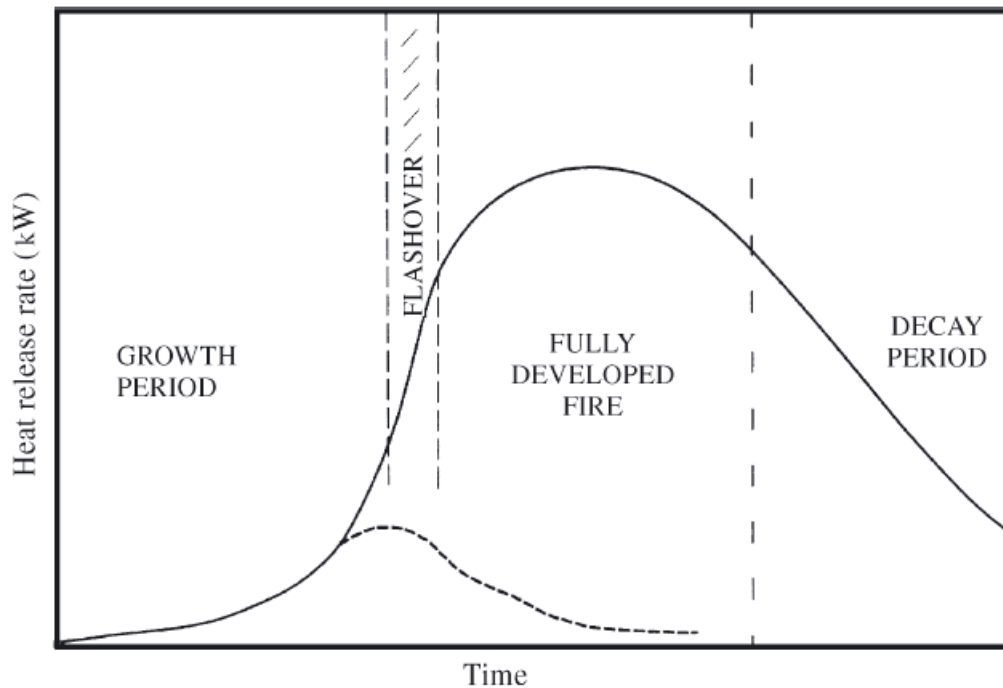
Figure 11: Typical heat release rate evolution for a compartment fire [34]

During the growth phase of a fire, the main hazard of combustible insulation materials is the onset of pyrolysis. Once released, pyrolysis gases may ignite very quickly and thus give an increased contribution of heat release in the compartment [18]. Also, since insulation materials reduce the heat losses in the compartment, time to flashover may decrease [34]. This can be seen from Figure 12, which shows that in scenarios with the same ventilation factor $A_w H^{1/2}$ and compartment dimensions 4m x 6m x 2.4m, the size of a fire sufficient to produce flashover is greatly reduced for highly insulating linings such as fibre insulating board or EPS [34].
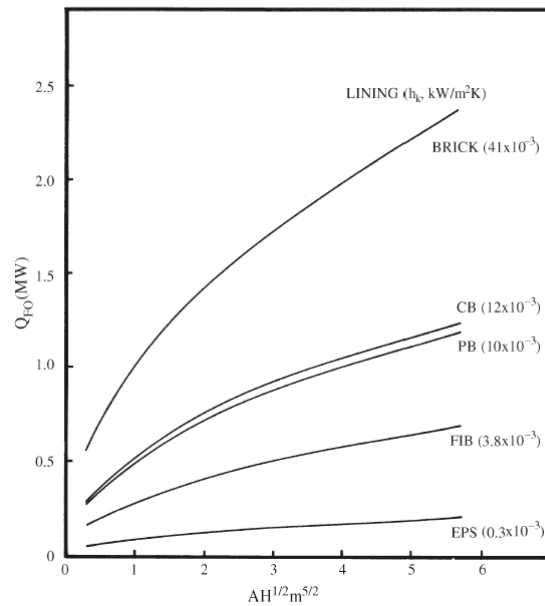
Figure 12: Heat release rate necessary for flashover in a compartment 4 m x 6 m x 2.4 m high as a function of $A_w H^{1/2}$ for different boundary materials [34]

The hazards created by the onset of pyrolysis during the pre-flashover stage of a fire will influence the available safe egress time (ASET), thus creating a risk when it comes to the safety of the building's occupants due to the short available time before untenable conditions are reached.

During the fully developed stage of a fire, the main hazard consists of the physical failure of the assembly, which could be damaged, making it possible for pyrolysis gases to be transported to other compartments. This could compromise evacuation if the gases escape towards egress routes, in case the installation of the compartment's barriers is not performed well, because of their toxicity as well as their ability to ignite, which would allow the fire to spread to other areas of the building.

To reduce or eliminate these hazards, assemblies which include insulation materials should be designed so that they can provide a fire safe use by delaying or stopping the onset of pyrolysis. This is done by ensuring that the insulation is not directly exposed to a fire by covering it with a lining with a higher thermal inertia, which will act as a thermal barrier. In this way, the onset of pyrolysis and ignition are delayed, and the time to flashover would not be reached as quickly, since the encapsulation will increase the heat losses from the compartment, in comparison with exposed insulation.

There are several frameworks that can be used to identify the failure criteria of insulation materials and assemblies in which they are contained. Currently, the main frameworks used for the design of insulation systems in fire rely on prescriptive codes, even though performance-based methodologies are being developed and increasingly allowed by some regulatory frameworks.

1.2.2.1 Prescriptive design

The EU regulatory framework is based on two sets of standards: BS EN 13501-1 [35], which gives a reaction-to-fire framework based on a flammability classification for products, and BS EN 1363-1 [36], which gives a fire-resistance framework [18].

8

The reaction-to-fire testing is aimed to reveal the likely contribution of materials to a pre-flashover fire, while the fire-resistance testing is aimed to reveal the likely fire spread in the subsequent stage to flashover, as well as the structural stability of loadbearing elements [18].

BS EN 13501-1 gives a classification, established on standard testing, of construction products based on how they contribute to a fire. This is translated into the different Euroclasses, which go from class A, for non-combustible materials, to class F for products which are unable to resist for a short period of time to a small flame attack without substantial fire spread.

The performance of a construction element is evaluated as a pass or fail of three criteria during standard fire-resistance tests [36]. These performance criteria are:

- mechanical strength (R), which is met when a structure can retain its load bearing capacity during the time of the fire. This criteria may not be relevant for most insulation systems [18].
- integrity (E), meaning that no openings through the structure should occur in case of a fire, which would allow hot gases or flames to pass through it, thus compromising compartmentation;
- thermal insulation (I) for the not exposed side, by not allowing a substantial temperature increase.

Integrity and insulation are the two criteria that allow for compartmentation. If either of those is compromised, this could induce a more severe fire spread throughout a building. Meeting these criteria is very important during the fully developed stage of a compartment fire to avoid fire spread.

However, results from standard fire testing do not necessarily represent real fires, and in some cases do not correspond to the most onerous scenarios and failure modes that might be experienced in a building [18]. This is because there are limits on the testing infrastructure, as well as the number of scenarios that can be performed. When it comes to testing insulation materials for R, E, I criteria, the results obtained from standard fire testing do not necessarily evaluate the main hazards, which are the contribution of heat release rate (HRR) and the generation and transport of toxic gases. Also, insulation materials are rarely exposed directly to flames, since they are placed behind a non-combustible lining, making their flammability assessment not representative of a real fire scenario [18].

1.2.2.2 *Performance-based design*
The purpose of a performance-based design in the case of insulation materials is to minimise the generation of pyrolysis gases in order to avoid heat release rate contributions to a fire. With this goal in mind, there are two potential design methodologies based on:

- defining a critical temperature (T_{cr}) to represent the onset of pyrolysis at the surface of the insulation material, thus setting a threshold value beyond which pyrolysis gases will become a hazard [37];
- defining the rate of pyrolysis gases for any potential heat exposure from a design fire, which would allow to the determine potential heat release increase in the compartment.

The critical temperature approach

The instant at which the surface of the material achieves the critical temperature is defined as the critical time, which depends on heat exposure of the assembly as well as on the material properties of the thermal barrier and the insulation [22]. If the insulation is not encapsulated by a lining material, this time can be obtained according to the following equation [37]:

$$\frac{T_{cr} - T_\infty}{T_C} = \left[1 - e^{\left(\frac{t_{cr}}{t_c}\right)} \cdot erfc\left(\left(\frac{t_{cr}}{t_c}\right)^{\frac{1}{2}} \right) \right] \tag{1}$$

where T_{cr} [K] is the critical temperature (equivalent to the pyrolysis onset temperature T_P), t_{cr} [s] is the critical time (equivalent to the pyrolysis onset time t_P), T_∞ is the ambient temperature [K], $erfc$ is the complementary Gaussian error function, T_C [K] is the characteristic surface temperature, and t_c [s] is the characteristic time. The last two parameters are defined as follows [37]:

$$T_C = \frac{\alpha \cdot \dot{q}_e^{"}}{h_T} \tag{2}$$

$$t_c = \frac{k\rho c}{(h_T)^2} \tag{3}$$

where α is the absorptivity of the exposed surface, $\dot{q}_e^{"}$ [W/m^2] is the external heat flux, h_T [W/m^{2}K] is the global heat transfer coefficient of losses, and $k\rho c$ [W^{2}s/K^{2}m^4] is the thermal inertia of the material. The global heat transfer coefficient of losses h_T can be defined as [37]:

$$h_T = h_{conv} + \varepsilon \cdot \sigma \cdot (T_P^2 + T_\infty^2) \cdot (T_P + T_\infty) \tag{4}$$

where h_{conv} [W/m^{2}K] is the convective heat transfer coefficient, ε is the emissivity of the surface, and σ [W/m^{2}K^4] is the Stefan-Boltzmann constant. The definition of the convective heat transfer coefficient is based on the estimation of the Nusselt number, which depends on the orientation of the surface with respect to the flow [37]:

$$\overline{Nu}_L = \frac{h_{conv} \cdot L_C}{k_{air}} \tag{5}$$

where k_{air} [W/mK] is the conductivity of air and L_C [m] is the characteristic length.

This methodology, classically used for defining simplified ignition models [38], is based on the transient heat transfer analysis of a semi-infinite solid, and it is thus only valid for one layer of insulation material which is directly exposed to a heat flux.

However, the goal for a fire safe use of insulation materials lies in assuring that the onset of pyrolysis is not achieved by its surface [22]. This can be done by encapsulating the insulation, with the goal to delay the arrival of the thermal wave to the insulation layer with the aid of a protective lining.

Assuming inert behaviour of the lining and the insulation material, the critical time can be predicted according to the following set of equations, which define the one-dimensional heat transfer problem consisting of two layers of materials [18]:

$$\dot{q}''_{net}(t) = -k_b \cdot \frac{\delta T}{\delta x}\Big|_{x=0^+} \quad \text{for } x = 0 \tag{6}$$

$$\frac{\partial \left(k_b \cdot \frac{\delta T}{\delta x}\right)}{\partial x} = \rho_b \cdot c_b \cdot \frac{dT}{dt} \quad \text{for } 0 < x < L_b \tag{7}$$

$$-k_b \cdot \frac{\delta T}{\delta x}\Big|_{x=L_b^-} = -k_i \cdot \frac{\delta T}{\delta x}\Big|_{x=L_b^+} \quad \text{for } x = L_b \tag{8}$$

$$\frac{\partial \left(k_i \cdot \frac{\delta T}{\delta x}\right)}{\partial x} = \rho_i \cdot c_i \cdot \frac{dT}{dt} \quad \text{for } L_b < x < L_b + L_i \tag{9}$$

$$-k_i \cdot \frac{\delta T}{\delta x}\Big|_{x=L_b+L_i} = \dot{q}''_{loss}(t) \quad \text{for } x = L_b + L_i \tag{10}$$

where $\dot{q}''_{net}$ [W/m^2] is the net heat flux at the surface of the lining, k_b and k_i [W/mK] are the thermal conductivity of the barrier and insulation respectively, ρ_b, ρ_i, c_b, c_i, L_b, and L_i indicate the density [kg/m^3], the specific heat capacity [J/kgK], and thickness [m] of both materials, and $\dot{q}''_{loss}$ [W/m^2] indicates the heat losses at the rear surface of the insulation. The heat losses depend on the back boundary conditions, thus by whether the insulation back layer is attached to another material or is directly exposed to air. Since the thermal inertia of an insulation material is low, the thermal wave would take longer to arrive to the back of the material, making $\dot{q}''_{loss}(t) = 0$ (adiabatic condition) a valid and conservative assumption [18]. Figure 13 shows the definition of this methodology.
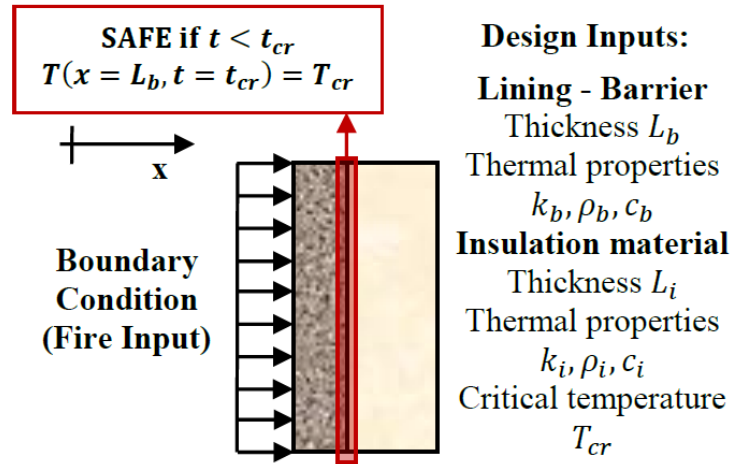
Figure 13: Schematics of the problem definition for a performance-based methodology to design fire safe insulated assemblies [22]

As suggested by Hidalgo et al. [37], for charring materials such as PIR or PF, the critical temperature can be defined through differential thermo-gravimetric analysis (DTG) under a nitrogen atmosphere at low heating rates and through Cone Calorimeter tests. The Cone Calorimeter test serves to determine the flammability properties of the insulation material, while DTG is used to assess the thermal degradation of the material. The critical temperature at the surface of the material could potentially be achieved prior to the ignition temperature, which can be quantified with the aid of the Cone Calorimeter. This is why information

regarding the thermal degradation mechanisms is essential for the interpretation of the critical temperature [37]. However, for materials with shrinking and melting behaviour such as EPS, this methodology for the determination of the critical temperature has been addressed as not suitable. Indeed, a more conservative approach was suggested by considering the melting temperature as the critical temperature [37]. The implications of this approach will be addressed in the following sections.

The critical temperature approach provides a conservative and simple methodology to find the critical time, which allows for a quantitative design to be performed in order to find fire safe solutions, thus even enabling the safe use of combustible insulation materials.

The pyrolysis modelling approach

A second approach for the characterisation of the hazard given after the onset of pyrolysis may be based the definition of a pyrolysis model which would be able to predict the thermal behaviour of the insulation material [39]. Computer pyrolysis models such as *Gpyro* are able to describe the thermal responses of solid materials exposed to radiative or convective heating [40]. However, these models are very complex, thus requiring a high number of input parameters and extremely competent trained users.

Recently, a simpler pyrolysis model based on a two-step uncoupled analysis has been proposed [41], which consists in isolating the heat transfer problem and the chemistry of the pyrolysis reactions. The heat transfer problem is solved in the first instance, followed by the estimation of the fraction of remaining mass and pyrolysis rates [41].

Once the heat transfer is solved, and thus the temperature of the material is known, the overall evolution of mass can be obtained for every time step j from the following equation [41]:

$$\bar{m}^j = \frac{\sum_{i=1}^{N}(\bar{m}_i^j \cdot \Delta x_i)}{L} \tag{11}$$

where $\bar{m}^j$ is the mass of the sample at the time step j, $\bar{m}_i^j$ is the normalised mass of the finite difference i, which is approximated directly as a function of the temperature $f(T)$, Δx_i [m] is the thickness of the *N* finite differences in which the space domain *L* [m] is divided.

The function $f(T)$ establishes the fraction of remaining mass, and is defined by direct reference to TGA results [39].

The mass loss rate per unit area [kg/m^{2}s] can then be obtained by deriving the mass loss rate over time and by considering the density of the material ρ_0 [kg/m^3] and the thickness of the sample *L* [m] [39]:

$$\dot{m}'^j_P = \rho_0 \cdot L \cdot \frac{\bar{m}^{j-1} - \bar{m}^j}{\Delta t} \tag{12}$$

Once the mass loss rate per unit area is found, a total rate of pyrolysis gas generation can be calculated as the sum from each of the exposure areas. Recent studies on PIR insulation have shown that this method can provide results with an acceptable degree of accuracy [39], which would allow further assessments of the potential heat release contribution [39], if the heat of combustion of those pyrolysis gases is known. Equivalently, the potential gaseous emissions could be obtained by multiplying the generation rate by the corresponding yields. As

proposed by Hidalgo et al., the failure time can then be defined as the time necessary to reach a critical value of heat release rate or emission concentration [39].

It is important to highlight that both approaches presented herein, while retaining a different level of complexity, have an application in engineering practice that is actually limited since a larger number of material parameter inputs would be required compared to the critical temperature approach.

1.2.3 Principles for an energy efficient design

The main objective from an energy efficiency point of view is to reduce the demand for energy in buildings for both cooling and heating. The main impact on this demand comes from the variation of outdoor temperatures, which has an influence on a building's internal temperature.

When the outdoor temperature drops during the night, the heat that flows outward from a wall more quickly compared to the heat that flows into a wall from the inside [42]. The heat flow outwards is maintained at the expense of the heat stored into the wall [42]. If a construction material has a high thermal capacity, represented as the product of thickness, density, and specific heat capacity, (i.e. bricks), its heat storage will be great, while the opposite is true for a material with a low thermal capacity. Once a rise in temperature occurs because of daylight, the outer portions of the wall store up the heat lost the night before [42]. This periodic heat flow through the wall can be translated into a transient-state approach.

When both indoor and outdoor conditions are stable, a steady-state approach can be considered. This type of approach can also be considered when the construction materials have a high thermal capacity, because of the high heat storage which can maintain indoor temperatures even with outdoor temperature variations. An example of this is given by traditional heavy brick buildings, which can cope with heat gains without having large inside temperature swings [43].

1.2.3.1 Steady-state approach

Most building components and structures are designed according to criteria and prescriptive thermal approaches derived from a steady-state thermal model [44], as requested by regulations such as *The Building Regulations 2010* in the UK. This model provides information regarding the energy needed to achieve an indoor comfort temperature when the effects of the heat flow into a building and out again cancel each other [20]. This is a condition averaged over a few days [20], when the building components have a high thermal capacity. This model is more precise when the daily temperature fluctuations remain within a narrow range [44], since these conditions would approximate more to a steady-state heat transfer regime.

An energy performance indicator that is often used is the thermal transmittance, or U-value. When assuming steady-state conditions, meaning that external and internal temperatures remain steady, the U-value is given by the following equation:

$$U = \frac{1}{R_{a-a}} \ [\text{W/m}^2\text{K}] \qquad (13)$$

where R_{a-a} is the air to air resistance [$\text{m}^2\text{K/W}$], which is the sum of the resistances of the surface and of the body of the element [45].

The R-value of any homogeneous layer is given by [45]:

$$R = \frac{L}{k} \ \ [\text{m}^2\text{K/W}] \tag{14}$$

where L is the thickness of the layer [m] and k is the thermal conductivity [W/mK].

The heat flow rate in case of a steady-state thermal model is given by the following equation [45]:

$$Q = A \ U \ \Delta T \ \ [\text{W}] \tag{15}$$

where A is the surface area of the layer [m^2], U is the thermal transmittance [W/m^{2}K], and ΔT is the mean yearly temperature difference between inside and outside.

However, there are only rare situations where environmental steady-state conditions occur, since external building conditions are affected by daily and seasonal cyclic temperature variations [44].

1.2.3.2 *Transient state approach*

Most meteorological variables show a regular variation which is repeated in a 24 hour cycle, called the periodic heat flow [45]. When the internal temperature of a building is affected by these periodic outside temperature variations, a transient state approach is best suited.

A model parameter for this approach can be derived from material properties such as density, specific heat capacity, and thermal conductivity. This parameter, classically called decrement factor, is the ratio of the cyclic transmittance u and the steady-state transmittance U:

$$f = \frac{u}{U} \tag{16}$$

This factor is able to quantify the mass effect of building systems. Building systems with a low thermal mass will have a decrement factor with a value close to 1, meaning that there is a higher heat gain/loss through the system [44].

The main heat input/output through a building system is given by gains and losses due to conduction, because this type of heat transfer is directly affected by daily and seasonal temperature variations [44]. A worst case scenario con be represented as a hypothetical day with maximum indoor-outdoor temperature difference and maximum outdoor temperature variation [44].

Then, the total conduction heat flow through a building system ($\dot{q}_{ee}$) can be evaluated as follows [44]:

$$\dot{q}_{ee} = \dot{q}_{ee,m} + \dot{q}_{ee,d} \tag{17}$$

$$\dot{q}_{ee,m} = A \cdot U \cdot \Delta T_m \tag{18}$$

$$\dot{q}_{ee,d} = A \cdot U \cdot f \cdot \frac{\Delta T_d}{2} \tag{19}$$

where $\dot{q}_{ee,m}$ [W] indicates the mean conduction heat flow driven by the mean monthly temperature difference between indoor and outdoor, $\dot{q}_{ee,d}$ [W] is the conduction heat flow due to daily temperature deviations from the outdoor daily mean, A [m] is the area in contact with the outdoor/indoor temperatures, U [W/m²K] is the thermal transmittance, ΔT_m [K] indicates the maximum mean monthly temperature difference between indoor and outdoor taken over a whole year, and ΔT_d [K] is the highest temperature variation from the mean temperature in one day.

1.3   Objectives

Construction design is a multi-criteria engineering problem, which comprises many variables such as energy efficiency, acoustics, cost, fire safety, and space limitations. Energy efficiency and sustainability have lately become the main drivers in building design, and this has led to the use of construction assemblies which contain insulation materials, many combustible, as shown in previous sections. Combustible materials tend to perform better from an energy efficiency and cost perspective due to their lower thermal conductivity, compared to non-combustible materials. However, combustible materials pose a fire hazard for the built environment.

As previously stated, current fire testing methodologies appear to not evaluate the main hazards generated by assemblies containing combustible insulation materials in a quantitative way that would allow for optimisation of performance design.

This multi-criteria problem is thus biased towards energy efficiency and cost, which can be quantitatively estimated, while fire safety is considered as a classification and a pass-fail criterion.

Given this issue, the aim of this thesis is to establish a framework for designing assemblies consisting of insulation materials based on performance principles of fire safety and energy efficiency, by achieving an integrated design that uses quantitative tools for both principles. This framework will enable the fire safe use of insulation materials in an integrated design approach, considering energy efficiency and cost/space reduction.

1.4   Scope

The analysis performed in this thesis is restricted to uniform construction systems such as SIPs, metal faced sandwich panels, and others which can be used as sub-systems in timber framed or masonry structures. Thermal bridges, joints, or studs are not taken into consideration. Different types of lining and insulation materials are used in order to demonstrate the applicability of the proposed methodology. Thus, the work presented herein is not intended to provide a set of solutions already applicable for design, but a framework available for designers that will allow them to design fire safe and energy efficient building systems containing insulation materials. Indeed, several material properties and assumptions are to be assessed when applying this framework.

2 Methodology

The methodology proposed to achieve the design of assemblies, both energy efficient and fire safe, is based on the use of the aforementioned quantitative tools or models that are able to establish the performance of different assembly configurations. From an energy efficiency perspective, the model, developed by following the CIBSE Guide, identifies the total conduction heat flow through an assembly. From a fire safety point of view, the model is developed by using the principles of heat transfer in order to find the critical time that indicates the onset of pyrolysis.

Figure 14 shows the proposed framework for the design of an assembly containing three layers which complies with both principles of energy efficiency and fire safety.
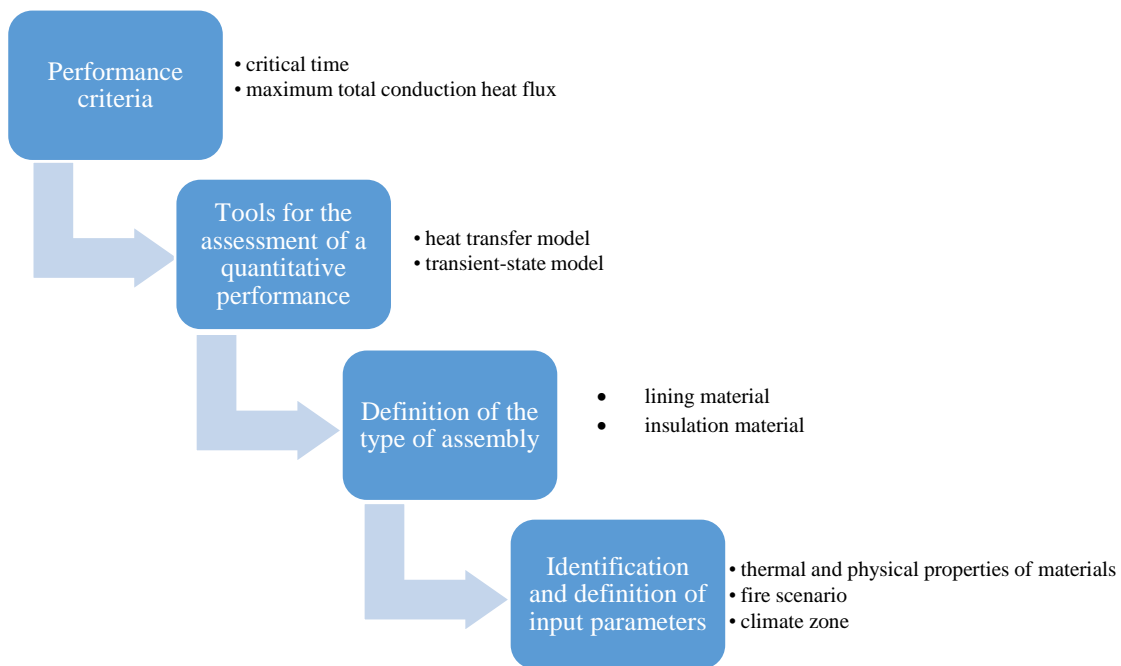
Figure 14: Methodology framework

These methodologies can be applied to a wide range of cases, as proven by the different fire scenarios, climate zones, and materials chosen as inputs.

Since the analysis presented in this thesis is simplified to specific assembly typologies, only considering lining and insulation and not the whole compartment area, the energy efficiency assessment is based on a heat flux ($\dot{q}''$ [W/m^2]) and not a heat flow ($\dot{q}$ [W]).

Assemblies containing three layers are analysed, with a lining-insulation-lining configuration. However, when looking at the fire safety of an assembly, the assumption that the boundary condition at the back of the insulation material is adiabatic is made. This means that no heat transfer will happen from that surface on. This assumption can be made because the thermal wave would take a time longer than the critical time to reach the back of the insulation material due to its low thermal inertia and thermal diffusivity.

In order to verify the validity of the methodology and its implications, i.e. whether the proposed models are conservative or not, results obtained analytically are also compared to results obtained in real tests. Due to the extended number of assumptions made to define these models, it is expected that the analytical results will not provide an accurate representation of reality. Whereas this is a clear limitation from a research perspective, the goal is to produce a robust, yet conservative, framework that would allow to incorporate quantitative criteria based on first principles for design purposes.

2.1 Performance criteria

The results obtained by the two models, which depend on the thermal and physical properties of each layer of the assembly, should be compared to performance criteria set from both the energy efficiency and fire safety point of view.

From the fire safety point of view, the criterion is established as the critical time, while from the energy efficiency point of view it is established as the total conduction heat flux through the assembly.

Since safe egress is a priority in case of fire, the critical time of an assembly must be higher than the required safe egress time. Assuming a worst-case scenario, the required evacuation time from a room with only one exit in buildings other than dwellings is 400 s, as shown in Appendix A, thus the critical time should be higher than this value. Similarly, as worst-case scenario, the required safe egress time from a dwelling house could be estimated as 120 s [46]. It should be noted that these values represent conservative scenarios to develop the methodology. However, designers should address specific required safe egress times for particular building geometries and scenarios.

As previously discussed, the performance criterion for energy efficiency is country dependent.

As a practical example, the UK set a target U-value in order to comply with the Nearly Zero Energy Buildings policy set by the European Union. This target U-value is 0.18 W/m²K for external walls in new dwellings [47], and 0.26 W/m²K for external walls in new buildings other than dwelling houses [48]. However, this target U-value only takes into account the steady-state case.

In order to be able to represent the transient-state as a performance criterion threshold, a decrement factor must be established. There are no guidelines on how to establish this factor, as this actually represents a decision of the designer. For the purpose of this thesis, a decrement factor equal to 1 is assumed, i.e. the cyclic transmittance (u) is equal to the thermal transmittance (U). This scenario implies an assembly that has a maximum conduction heat flux for each climate zone, above which the energy efficiency target is not met. The calculation for the total conduction heat flux is given by the following equation:

$$\dot{q}''_{ee} = U \cdot \Delta T_m + U \cdot f \cdot \frac{\Delta T_d}{2} \tag{20}$$

Table 1 shows the critical (maximum permitted) values of total conduction heat flux for an assembly in different climate zones to meet the criteria established by the assumptions presented above, i.e. U-value set by UK standards and a simplified decrement factor. The selection of climate zones will be further detailed in section 2.4.2.

Table 1: Established critical total conduction heat flux for different climate zones

Zone	$\dot{q}''_{ee,m}$ [W/m²] Dwellings	$\dot{q}''_{ee,d}$ [W/m²] Dwellings	$\dot{q}''_{ee,m}$ [W/m²] Other than dwellings	$\dot{q}''_{ee,d}$ [W/m²] Other than dwellings	$\dot{q}''_{ee,max}$ [W/m²] Dwellings	$\dot{q}''_{ee,max}$ [W/m²] Other than dwellings
2	1.4305	0.9284	2.0664	1.3409	2.3589	3.4073
4	1.6605	1.3237	2.3985	1.9120	2.9842	4.3105
7	2.2302	0.8442	3.2214	1.2194	3.0744	4.4408

When designing assemblies which should also be energy efficient, the designer should apply a transient-state approach by taking into consideration the type of building, the climate zone and the maximum critical heat losses to be assumed. The critical heat losses is an arbitrary value, however designers could decide an adequate value based on the heat loads of the building and the HVAC system.

2.2 Tools to assess performance

The models, which are set to assess the performance of a three-layer assembly, provide quantitative results. They are subsequently compared based on the performance criteria parameters previously set.

2.2.1 Fire safety model

The fire safety model, developed via *Matlab*, provides the critical temperature of an assembly consisting of two layers. Only two layers are modelled because of the assumption that the boundary condition at the back of the insulation material is adiabatic.

The used modelling technique for solving the one-dimensional conduction heat transfer problem through the two layers is based on the finite differences techniques presented by Hidalgo [8], which corresponds to a Crank-Nicolson method (second-order method in time, implicit in time, and numerically stable). Figure 15 shows the discretisation for a composite sample consisting of two layers of different materials, assuming no thermal contact resistance.
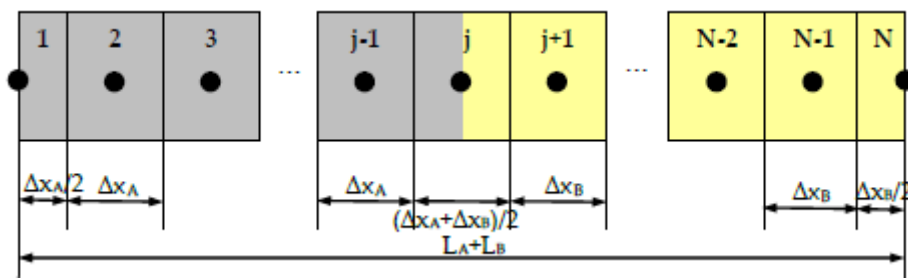
Figure 15: Discretisation of the space domain for the one-dimensional heat transfer problem consisting of two layers [8]

Since a Crank-Nicolson method is used, the temperature of each finite difference element is obtained for each time step j and each element i as:

$$T_i^{j+1} = T_i^j + \frac{\Delta t}{2}\left(\frac{\partial T_i^j}{\partial t} + \frac{\partial T_i^{j+1}}{\partial t}\right) \tag{21}$$

A system of equations can be obtained by constructing each discretised governing equation for boundary conditions at the front and back surface, and for interior and interface elements as a function of the rate of temperature change $\frac{\partial T_i^j}{\partial t}$.

The discretised governing equation for the boundary condition at the surface at the time step j can be derived from applying an energy balance between the external conditions and elements 1 and 2 [8]:

$$\dot{q}''^j_{net} = \dot{q}''^j_{st,1} + \dot{q}''^j_{1\rightarrow 2} \tag{22}$$

where $\dot{q}''^j_{net}$ is the net heat flux at the surface, $\dot{q}''^j_{st,1}$ is the heat flux stored by the first element, and $\dot{q}''^j_{1\rightarrow 2}$ is the heat flux conducted from element 1 to element 2. j represents the step in the equation.

Equation 22 can be rewritten as:

$$\alpha\dot{q}''_e - h_T\left(T_1^j - T_\infty\right) = \rho c_p \frac{\Delta x}{2}\frac{\partial T_i^j}{\partial t} + k\frac{(T_1^j - T_2^j)}{\Delta x} \tag{23}$$

where α is the absorptivity of the surface material, which for this work is assumed as 0.8 (this is an average value for greybody radiation), $\dot{q}''_e$ is the radiant heat flux, and h_T is the heat transfer coefficient of losses.

For the model, the assumption is made that the heat flux set as input is equal to $\dot{q}''_e$, while for the heat transfer coefficient of losses, only radiative losses are taken into consideration:

$$h_T = \varepsilon\sigma T^3 \tag{24}$$

where the emissivity of the materials can be generally assumed equal to the absorptivity $\varepsilon = 0.8$ and σ is the Stefan-Boltzmann constant $\sigma = 5.67 \cdot 10^{-8}$ W/m²K⁴. This assumption can be justified by the fact that at high temperatures radiative heat losses dominate over convective losses [23], and still would provide a conservative approach. It should be noted that the convective coefficient depends on the length scale of the system, as shown in Equation 5. Since no geometry has been established for this framework, a conservative decision has been made by neglecting the convective coefficient. The error given by this assumption will be assessed in following sections.

For the interior elements of both material layers, assuming that the conductivity is constant, the discretised equation can be defined as:

$$\dot{q}''_{i-1\to i} = \dot{q}''_{i,st} + \dot{q}''_{i\to i+1} \tag{25}$$

where j represents the step, and i represents the element. Equation 25 can be written as:

$$k\frac{(T^j_{i-1} - T^j_i)}{\Delta x} = \rho c\frac{\partial T^j_i}{\partial t}\Delta x + k\frac{(T^j_i - T^j_{i+1})}{\Delta x} \tag{26}$$

At the interface between the two different layers, the governing equation is the same as Equation 25, given that thermal contact resistance is disregarded. However, since at the interface there are different material properties, this equation can be written as:

$$k_A\frac{(T^j_{i-1} - T^j_i)}{\Delta x_A} = (\rho_A c_A \frac{\Delta x_A}{2} + \rho_B c_B \frac{\Delta x_B}{2})\frac{\partial T^j_i}{\partial t} + k_B\frac{(T^j_i - T^j_{i+1})}{\Delta x_B} \tag{27}$$

where A indicates the first material layer and B the second material layer.

Finally, for the last element, the discretised equation can be derived by applying an energy balance at the rear face [8]:

$$\dot{q}''_{N-1\to N} = \dot{q}''_{N,st} + \dot{q}_{loss} \tag{28}$$

As previously explained, the assumption of an adiabatic back surface of the insulation material gives $\dot{q}_{loss} = 0$.

Figure 16 shows the iterative process required to solve the heat transfer problem formulated in Equations 21 to 28, by using a Crank-Nicolson method. The outcome of the model provides the temperature evolution through the whole assembly. With these results it is possible to obtain the critical time at which the surface of the insulation material (interface lining-insulation) reaches its critical temperature, by checking at every time step if this critical temperature has been reached. This method can be expressed by the following equation:

$$T(x = L, t_{cr}) = T_{cr} \tag{29}$$
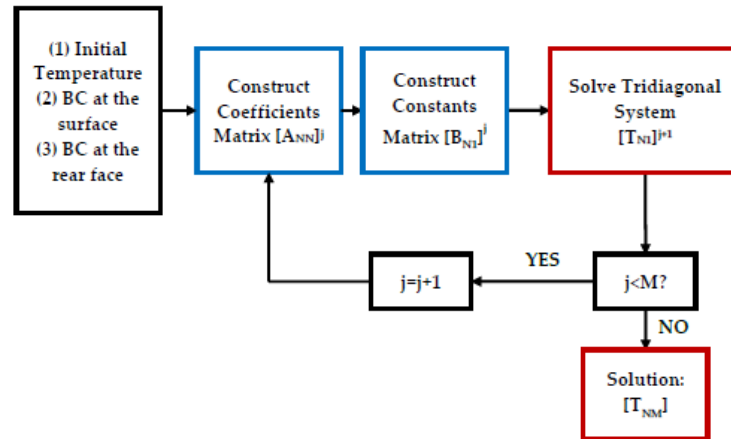
Figure 16: Diagram for the determination of the temperature's map for a domain consisting of N elements and M time steps
[8]

2.2.2 Energy efficiency model

The energy efficiency model was constructed by following the Chartered Institution of Building Services Engineers (CIBSE), Guide A [49], along with the model proposed by Soret et al. [44], which includes not only a steady-state approach, but also a transient-state one. The procedure of the method assumes that all internal and external load fluctuations can be represented by the sum of a steady-state component and a sine wave with a period of 24 h [49].

When considering a transient-state approach, the two variables that are needed are the U-value and the decrement factor, which depends on the cyclic transmittance, as well as the U-value.

The U-value for an assembly containing three layers is given by the following equation:

$$U = \frac{1}{R_{si}} + \frac{k_A}{L_A} + \frac{k_B}{L_B} + \frac{k_C}{L_C} + \frac{1}{R_{se}} \tag{30}$$

where R_{si} is the resistance of the surface adjacent to the internal environment, and is assumed equal to 0.13 m^{2}K/W, and R_{se} is the resistance of the surface adjacent to the external environment, and is assumed equal to 0.04 m^{2}K/W [50]. The letters A, B, C refer to each of the different materials that are part of the assembly. In this case materials A and C are considered to be the same.

For a multi-layered assembly, the cyclic transmittance is found by solving a system of matrices which presents the relation between the surface values, which are a function of the thickness of each material, as well as their thermal conductivity, density, and specific heat capacity. When an assembly is made out of three layers, these matrices can be written as [20]:

$$\begin{bmatrix} T_1 \\ q_1 \end{bmatrix} = \begin{bmatrix} e_{11} & e_{12} \\ e_{21} & e_{22} \end{bmatrix} \begin{bmatrix} f_{11} & f_{12} \\ f_{21} & f_{22} \end{bmatrix} \begin{bmatrix} g_{11} & g_{12} \\ g_{21} & g_{22} \end{bmatrix} \begin{bmatrix} T_4 \\ q_4 \end{bmatrix} \tag{31}$$

where e_{jk} denotes the complex elements of the first layer, and f_{jk} those of the second layer.

The overall quantities can be related by multiplication of a sequence of such matrices to form the wall matrix with elements e'_{jk} [20]:

$$\begin{bmatrix} T_i \\ q_i \end{bmatrix} = \begin{bmatrix} e'_{11} & e'_{12} \\ e'_{21} & e'_{22} \end{bmatrix} \begin{bmatrix} T_o \\ q_o \end{bmatrix} \tag{32}$$

The cyclic transmittance u [W/m^{2}K] is then given by [20]:

$$u = \left[\frac{q_i}{T_o} \right]_{T_i=0} = \frac{-1}{e'_{12}} \tag{33}$$

where q_i indicates the heat flow at the inside surface, T_o the outside temperature, and T_i is the inside temperature. $T_i = 0$ means that the internal surface is taken to be isothermal [20].

For each layer, a matrix is made with its e_{jk} elements in the following way [49]:

$$\begin{pmatrix} m_1 & m_2 \\ m_3 & m_4 \end{pmatrix} = \begin{pmatrix} \cosh(\tau + i\tau) & \dfrac{L \cdot \sinh(\tau + i\tau)}{k \cdot (\tau + i\tau)} \\ \dfrac{k \cdot (\tau + i\tau) \cdot \sinh(\tau + i\tau)}{L} & \cosh(\tau + i\tau) \end{pmatrix} \quad (34)$$

where, for a 24-hour cycle, the cyclic thickness τ represents the way a thermal wave travels through the system, and is given by the following equation [20]:

$$\tau = \left(\frac{\pi \cdot \rho \cdot c}{P \cdot k} \right)^{\frac{1}{2}} \cdot L \quad (35)$$

where ρ is the density of the material [kg/m^3], c is the specific heat capacity of the material [J/kgK], L is the thickness of the layer [m], k is the thermal conductivity of the material [W/mK], and P is the periodic time [s], which, for a daily temperature variation is $P = 24 \cdot 3600 = 86400 \ s$

A value of τ of about 0.1 or lower represents a "thin" wall, in the sense that there can be little temperature difference across it. A τ value larger than 3 represents a wall that is considered "thick", meaning that excitation at surface 1 has little effect at surface 2 [20].

For a composite wall, the matrices of each layer are multiplied in the same order as the one in the physical assembly [20], meaning that the matrix of the first layer is multiplied to the one of the second layer, and their product is multiplied to the matrix of the third layer.

Once the thermal and the cyclic transmittance are obtained, it is possible to find the decrement factor as:

$$f = \frac{u}{U} \quad (36)$$

Once the decrement factor is found for a particular assembly, the total conduction heat flux can be calculated by using Equation 20.

2.3   Assembly typologies

The assemblies taken into consideration contain two layers of lining material, which encapsulate one layer of insulation. Thermal bridges, joints, or studs are not taken into consideration, thus the analysis is performed only on uniform construction systems.

The selected encapsulation layers are made of either magnesium oxide boards (MgO), brick or plasterboard, which correspond to typical lining materials found in the built environment. The second layer comprises the insulation material, for which is either EPS, PIR or PF are selected. For the final purpose of comparing assemblies consisting of combustible and non-combustible insulation, assemblies including stone wool are also selected. Each layer is analysed at different thicknesses, presented in Table 2, in order to see the role that the thickness of each layer plays in meeting the performance criteria. The selected thickness correspond to typical values provided by manufacturers.

Material	MgO[51]	Brick[33][52][53]	Plasterboard[54][55]	Insulation[56] (EPS/PIR/PF/Stone wool)
Thickness [mm]	3	65	9.5	92
	4	76	10	144
	5	79	12.5	188
	6	90	13	238
	7	92	15	289
	8	103	16	
	9	110		
	10			
	12			
	14			
	15			
	16			
	18			
	20			
	24			
	30			
	38			
	45			
	50			

2.4   Methodology Inputs

Both computational models need inputs regarding the physical and thermal properties of the materials enclosed in the assembly. As presented above, for the lining, those materials are: magnesium oxide board, brick, and plasterboard. When it comes to the insulation materials, those that are analysed are: EPS, PIR, and PF. Table 3 and Table 4 give the needed properties of each material. These are standard properties measured at ambient temperature, typically provided by manufacturers.

Table 3: Properties of insulation materials at ambient temperature [37]

Material	Thermal conductivity k [W/mK]	Density ρ [kg/m³]	Specific heat capacity c [J/kgK]	Critical temperature [°C]
EPS	0.038	10	1500	240
PIR	0.028	32	1500	300
PF	0.024	38	1500	425

Table 4: Properties of lining materials at ambient temperature

Material	Thermal conductivity k [W/mK]	Density ρ [kg/m³]	Specific heat capacity c [J/kgK]
MgO	0.32 [57]	974	1074
Plasterboard	0.17[58]	800[58]	1090[59]
Brick	1.31[22]	2000[22]	921[22]

The value of the density of MgO indicated in Table 4 is an average value taken from four different samples, while the specific heat capacity was found with a Transient Plane Source Sensor (TPS) (Andy Wong, the University of Queensland, personal communication, February 2017).

Each lining material is analysed at different thicknesses, as indicated in Table 2. These thicknesses are chosen according to the real use of each material.

2.4.1 Fire safety inputs

When analysing an assembly from a fire safety point of view, the main variable is represented by the thermal boundary condition at the surface of the assembly, which is defined by the heat flux to which the assembly is exposed to. The thermal boundary condition at the surface of a structure in a fire can be defined as:

$$\dot{q}''_{net} = \dot{q}''_{rad} + \dot{q}''_{conv} \tag{36}$$

where $\dot{q}''_{net}$ is the net heat flux conducted at the surface of the solid, $\dot{q}''_{conv}$ is the net convective heat flux, and $\dot{q}''_{rad}$ is the net radiative heat flux. This boundary conditions expression can be generally defined as [60]:

$$\dot{q}''_{net} = \alpha \cdot q''_{inc} + h_c(T_g - T_s) - \varepsilon \sigma T_s^4 \tag{37}$$

where α is the absorptivity, is $\dot{q}''_{inc}$ the incident radiant heat flux, h_c is the convective coefficient of losses, T_g is the gas temperature, T_s is the surface temperature, ε is the emissivity, and σ is the Stefan-Boltzmann constant.

Each fire scenario may be described with a different external heat flux curve, thus infinite scenarios could be considered. Since the main hazard from a fire safety point of view is the onset of pyrolysis of the insulation material, it is important to analyse pre-flashover scenarios, when safe egress is the priority. Post-flashover scenarios are also analysed, in case of failure of the compartment's barriers which allow pyrolysis gases to possibly move towards evacuation routes. This failure could be caused by bad practice in constructing, joining, or sealing of the installation [18].

For the purpose of this thesis, two representative scenarios of a pre-flashover fire, and three of a post-flashover fire were chosen. Each representative scenario has a different peak heat flux, and a different evolution over time.

The considered pre-flashover scenarios correspond to two constant heat fluxes expected from a single burning item (SBI) test [61], obtained from well-ventilated tests in a corner fire configuration, which is considered to be a potential worst-case scenario because the burning item is very close the walls, thus obtaining flame impingement [62]. The constant heat fluxes that are analysed are the ones that are the closest to the single burning item, thus 30 kW/m² and 35 kW/m², as can be seen from Figure 17.
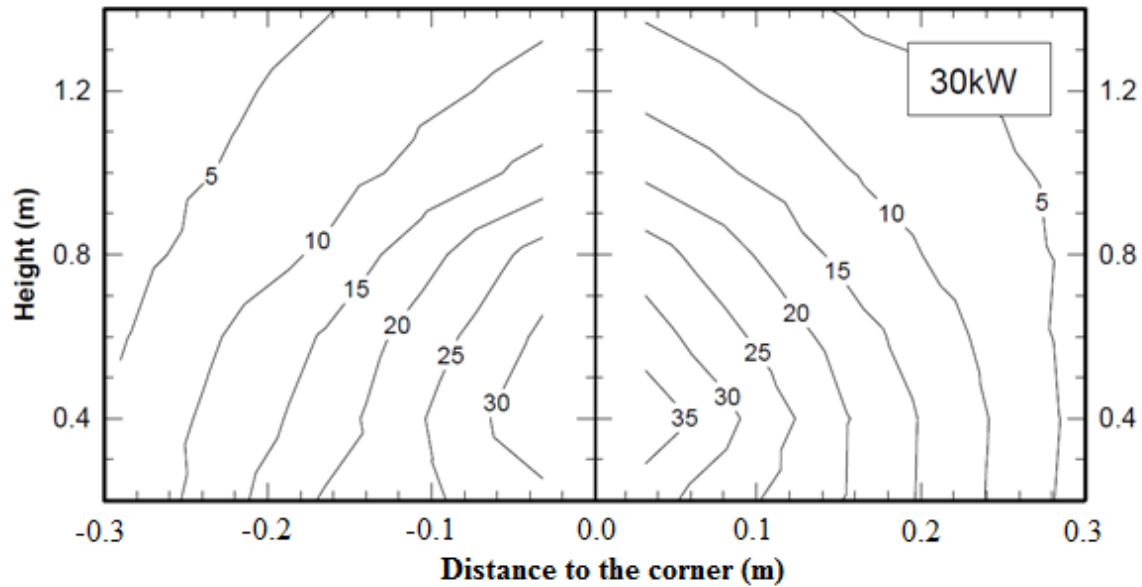
Figure 17: Distributions of the derived surface heat flux on the left and right panels tested to the Single Burning Items test [62]

Figure 18 shows the evolution of the heat flux over time measured onto a wall of a compartment during the Cardington large scale fire test with a fuel load made out of 80% wood and 20% plastic materials, representing a post-flashover scenario [63].
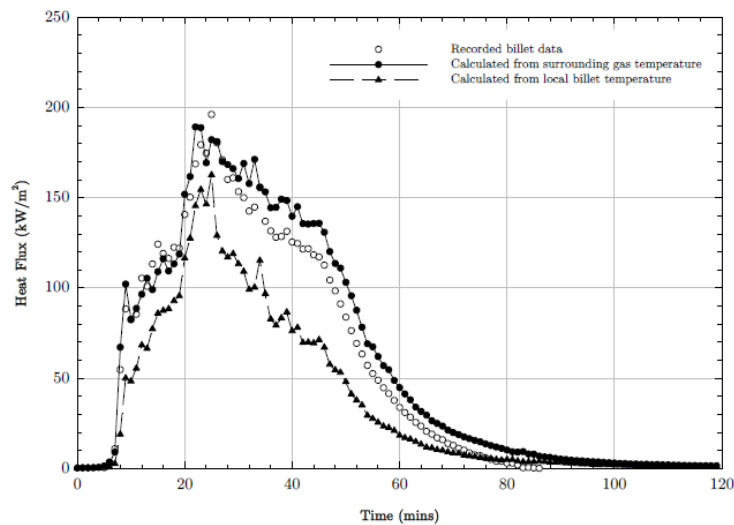
Figure 18: Heat fluxes recorded and calculated from the relevant true gas temperature and the local surrounding gas temperature [63] [64]

The second post-flashover heat flux curve that is analysed, shown in Figure 19, is the standard fire total gauge heat flux, calculated for the same compartment as the previously mentioned one, according to the Eurocode standard fire curve [63].
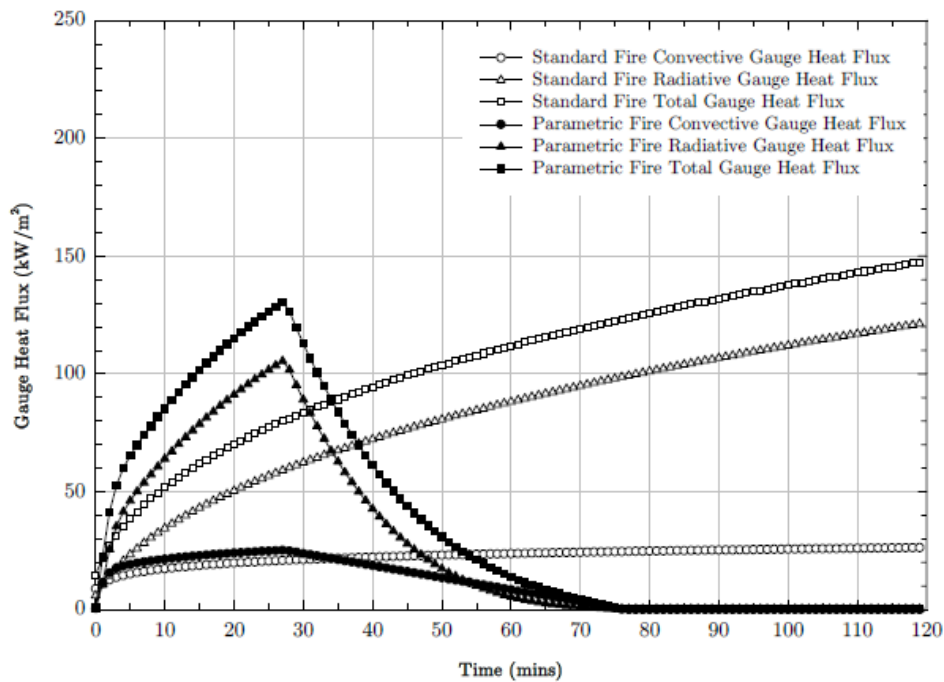
Figure 19: Convective, radiative and total gauge heat fluxes expected within the compartment as a result of the Eurocode parametric and standard fires [63]

The last analysed post-flashover scenario is the heat flux curve registered by the thin skin calorimeter (TSC) during a medium-scale timber compartment fire test, shown in Figure 20. The compartment was made of cross laminated timber panels, where TSCs were placed each at one side of the of the compartment [65].
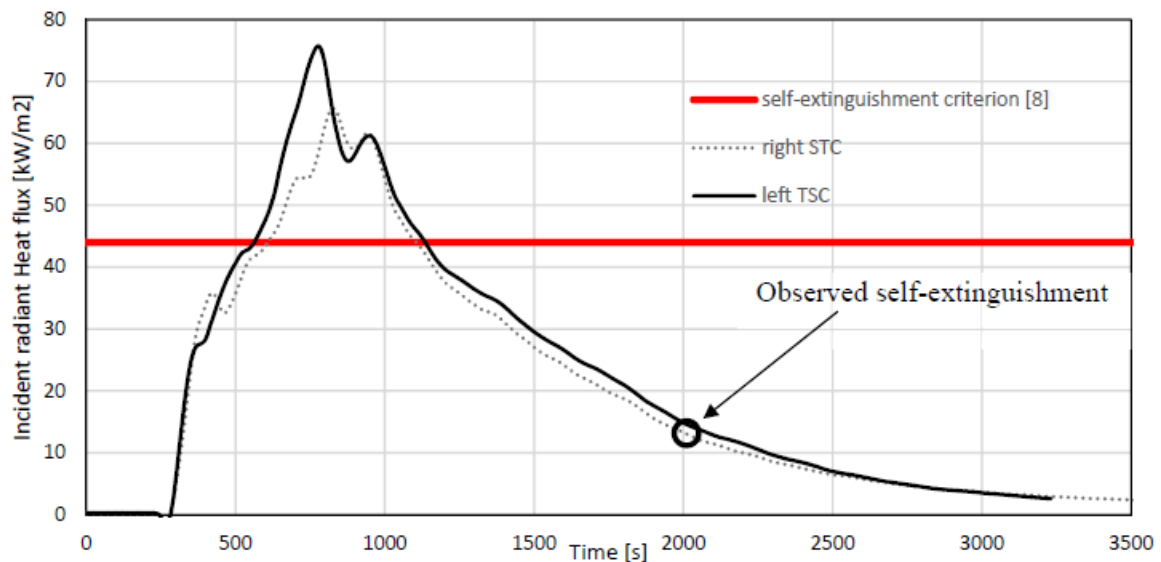
Figure 20: Incident radiant (external) heat flux obtained from thin skin calorimeters [65]

2.4.2 Energy efficiency inputs

To analyse the energy efficiency of an assembly, the variables that need to be quantified are the monthly and daily temperature variations. Three different Australian climate zones are analysed:

- zone 2, with a warm humid summer and a mild winter, is the climate zone where Brisbane is located;
- zone 4, with a hot dry summer and a cool winter, which also represents the Mediterranean climate;
- zone 7, with a cool temperate climate, such as the one in the United Kingdom.

The complete list and location of the Australian climate zones can be found in Appendix B.

The maximum temperature difference between the monthly mean and the thermal neutrality (ΔT_m) and the historical mean daily temperature variations (ΔT_d) for each zone are given in Table 5.

Table 5: Temperature variations for Australian locations [44]

| Climate Zone	Australian location	$\Delta T_m[°C]$	$\Delta T_d[°C]$
2	Rockhampton Aero QLD	6.32	11.70
	Brisbane Aero QLD	7.28	9.73
	Toowoomba Airport QLD	9.70	10.49
	Coffs Harbour MO NSW	8.49	9.34
4	Murchison WA	8.22	15.93
	Wiluna WA	9.04	14.89
	Oodnadatta Airport SA	8.84	14.49
	Mildura Airport VIC	10.80	13.52
7	Canberra – Tuggeranong (Isabella Plains) AWS ACT	13.36	13.88
	Cape Sorell TAS	11.08	5.48
	Hobart Airport TAS	11.87	9.44
	Scotts Peak Dam TAS	13.25	8.72

For simplification purposes, an average value of the temperature difference for every zone is used, in order to have one input per zone. These input values are shown in Table 6.

Table 6: Average temperature variations

Climate Zone	ΔT_m [°C]	ΔT_d[° [°C]
2	7.95	10.32
4	9.23	14.71
7	12.39	9.38

2.5 Methodology validation

Whereas the models proposed for this work are based on sound first principles and peer reviewed literature, this methodology carries a series of assumptions and limitations that need to be assessed, since these could yield to non-conservative or artificial results. Nonetheless, the validation process is a delicate process in which reliable experimental data is required.

For most cases, validation data are limited due to poor definition of the boundary conditions or poor density of the instrumentation. For the purpose of this thesis, some experimental data are assessed but clear limitations are identified in this process. Uncertainties of these methods will be revised in further sections.

2.5.1 Energy efficiency model

R-, and thus U-values of assemblies can be validated with the standardized Hot Box test [66]. Soret et al. [66] have performed further validations of this parameter based on an alternative method based on radiant heaters (lamps). Both methods have shown sufficient capabilities to represent the thermal behaviour of the system based on proposed certified U-values from manufacturers. Validation of the transient process represented by the decrement factor is, however, a more complex scenario; unfortunately limited literature was found on this matter. As shown in Table 1, the heat flux due to transient behaviour is not negligible, especially for those cases with a decrement factor close to 1. A validation is therefore necessary to corroborate the assumptions proposed by the methodology suggested by the CIBSE guide. This is however out of the scope of this thesis, and further work should aim at establishing the range of validity of this method, along with the expected errors.

2.5.2 Fire safety model

The heat transfer model was attempted to be validated by comparing the obtained results with experimental data, from both literature sources, and an experiment performed for the purpose of this work.

The experiment was performed on a SIP made out of two MgO linings, one on each side, and a core of EPS, as shown in Figure 21 and Figure 22. A thermal bridge made of MgO is present in the middle of the sample, which has a higher thermal inertia compared to the surrounding material, thus reducing the actual thermal performance of the SIP.

Figure 21: SIP sample used for the test
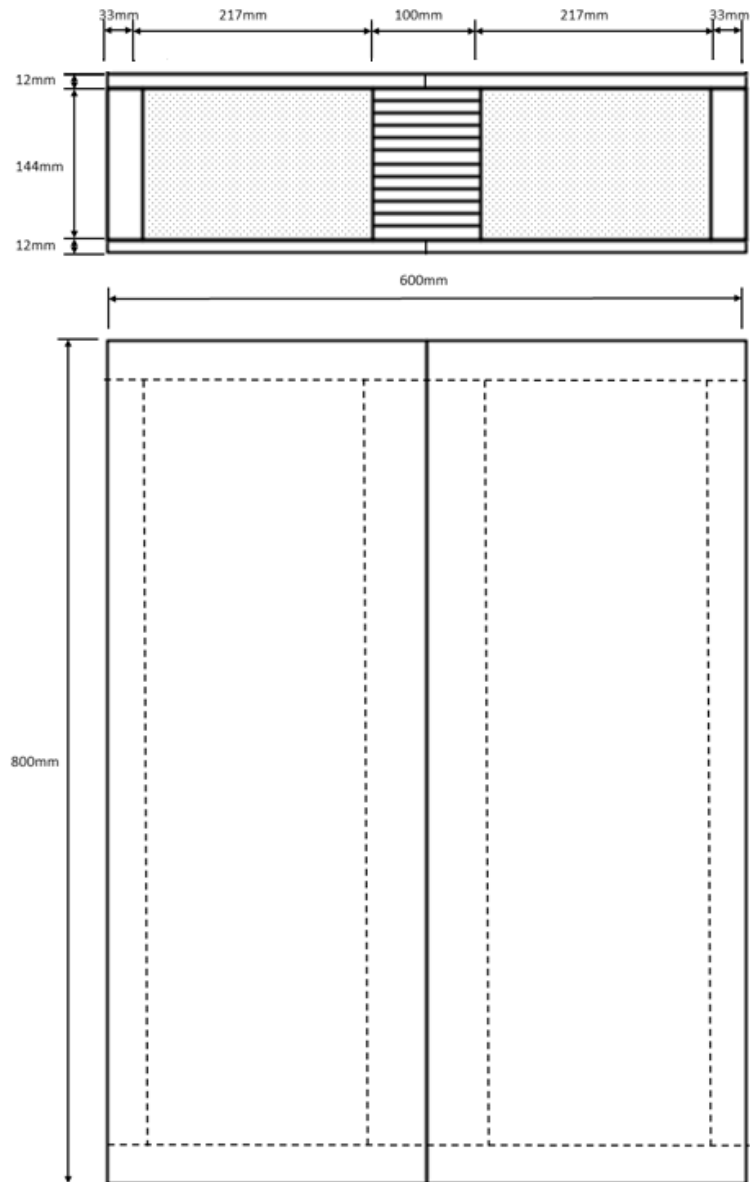
Figure 22: Measurements of the SIP sample

The sample was placed 90 mm away from a radiant panel, in order to achieve the highest heat flux possible from a single panel, as shown in Figure 23. This maximum heat flux consisted of a value of 65 kW/m², which was found by performing a heat flux mapping.
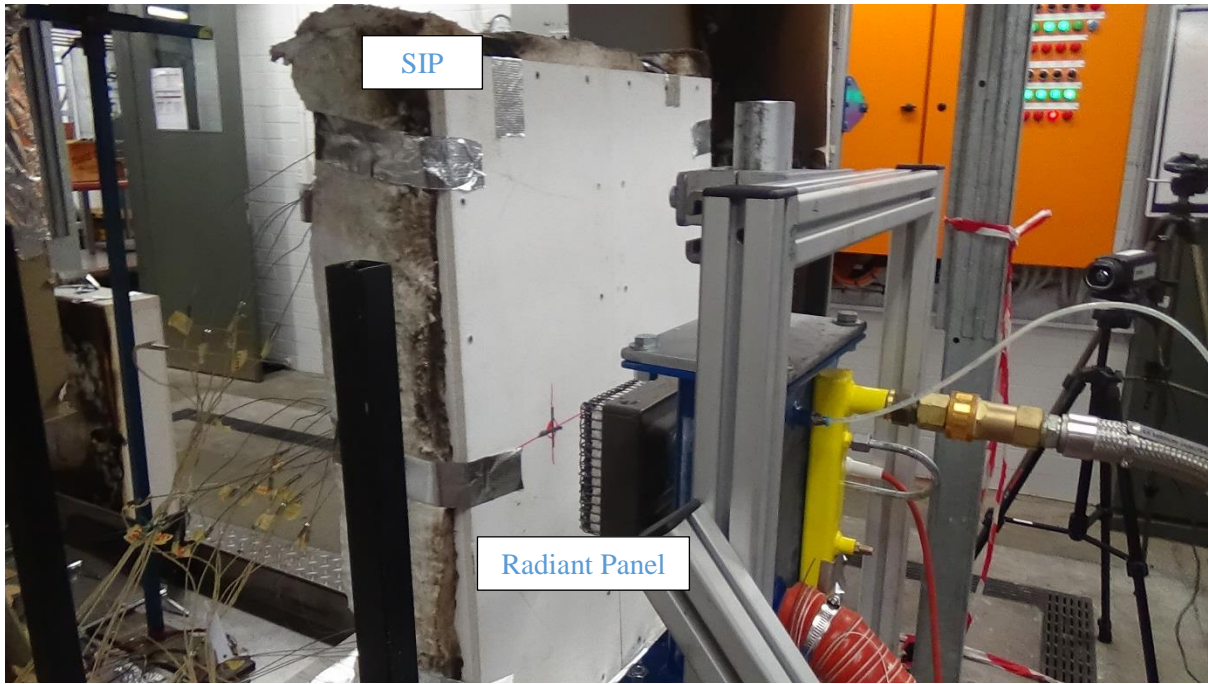
Figure 23: Placement of the sample in front of one radiant panel

Thermocouples were inserted on the back of each sample at different depths and heights, to measure the temperature in each material at different positions, as shown in Figure 24 to Figure 26.
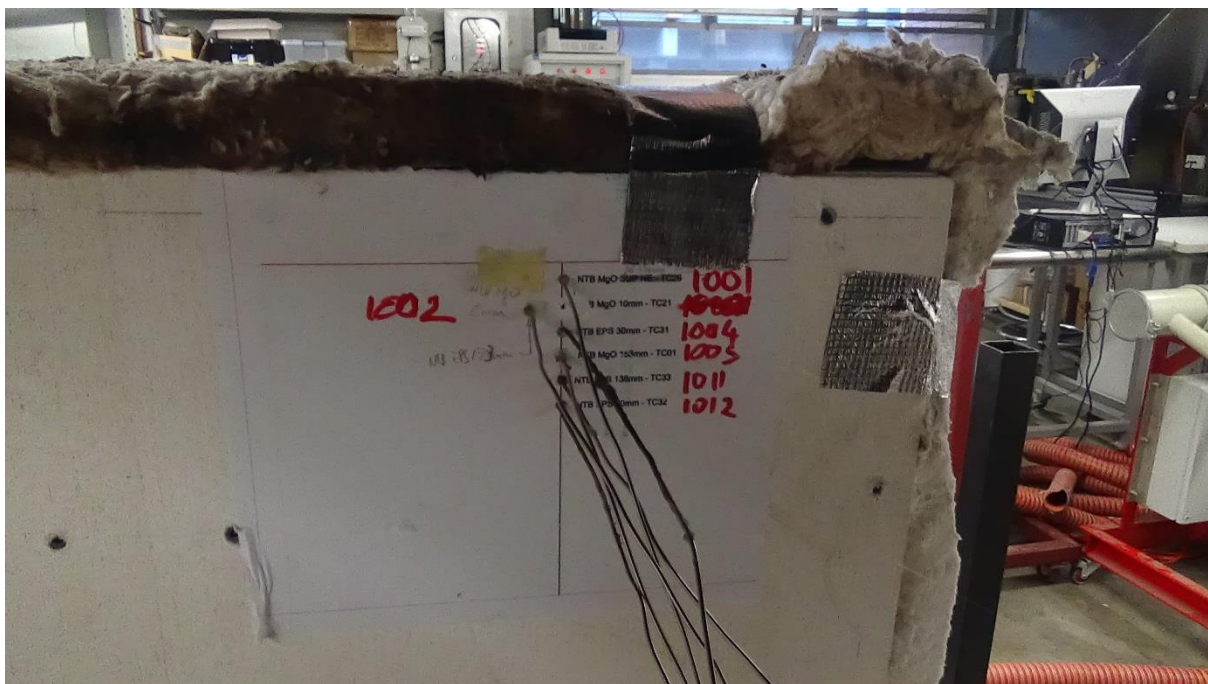
Figure 24: Close up of upper thermocouples
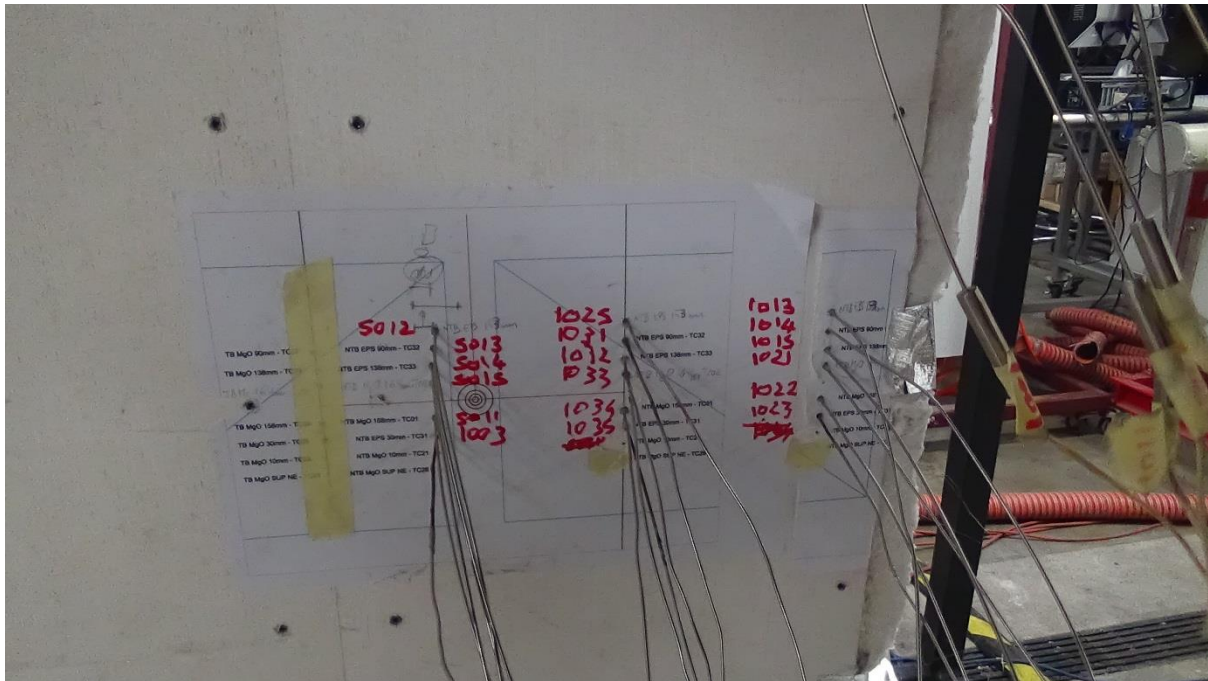
Figure 25: Close up of central thermocouples

Figure 26: Close up of lower thermocouples

Table 7 shows the exact position of each thermocouple inside the sample. An example of how the thermocouples are placed inside the sample can be seen in Appendix C.

Table 7: Thermocouple placement

Thermocouple	Depth [mm]	Material
1001	164	MgO
1002	153	EPS

1004	30	EPS
1005	158	MgO
1011	138	EPS
1012	90	EPS
1013	153	EPS
1014	90	EPS
1015	138	EPS
1021	164	MgO
1022	158	MgO
1023	30	EPS
1025	153	EPS
1031	90	EPS
1032	138	EPS
1033	164	MgO
1034	158	MgO
1035	30	EPS
5012	153	EPS
5013	90	EPS
5014	138	EPS
5015	164	MgO
5011	158	MgO
1003	30	EPS
5031	90	EPS
5032	138	EPS
5033	158	MgO
5034	30	EPS
1024	153	EPS

3   Results

The energy efficiency and fire safety models are applied to 7200 scenarios consisting of different combinations of inputs (lining and insulation materials, thickness of both layers, climate zone, and heat flux exposure). All the combinations are run with the inputs taken from Table 2, Table 3, Table 4, Table 6, Figure 17, Figure 18, Figure 19, and Figure 20.

Each case has as results both the critical time (t_{cr}) for the insulation material to reach its critical temperature at the surface, and the total conduction heat flux through the assembly ($\dot{q}''_{ee}$).

It is important to notice that, due to the formulation of the problem, the critical time does not depend on the thickness of the insulation material; when scenarios were run where the thickness of the insulation changed, the results obtained were the same for all different thickness. This is because the critical time for the insulation material to reach the critical temperature at its surface is generally much shorter than the time for the thermal wave to reach the back face of the insulation, thus making its thickness a negligible input variable for the fire safety assessment.

Figure 27 shows the results for each scenario, differentiating for the cases of each combustible insulation material (EPS, PF, and PIR). The scenarios which have an infinite critical time, meaning that the insulation material never reaches its critical temperature for the considered period of heat exposure, are assigned a critical time of 8000 s for plotting purposes.
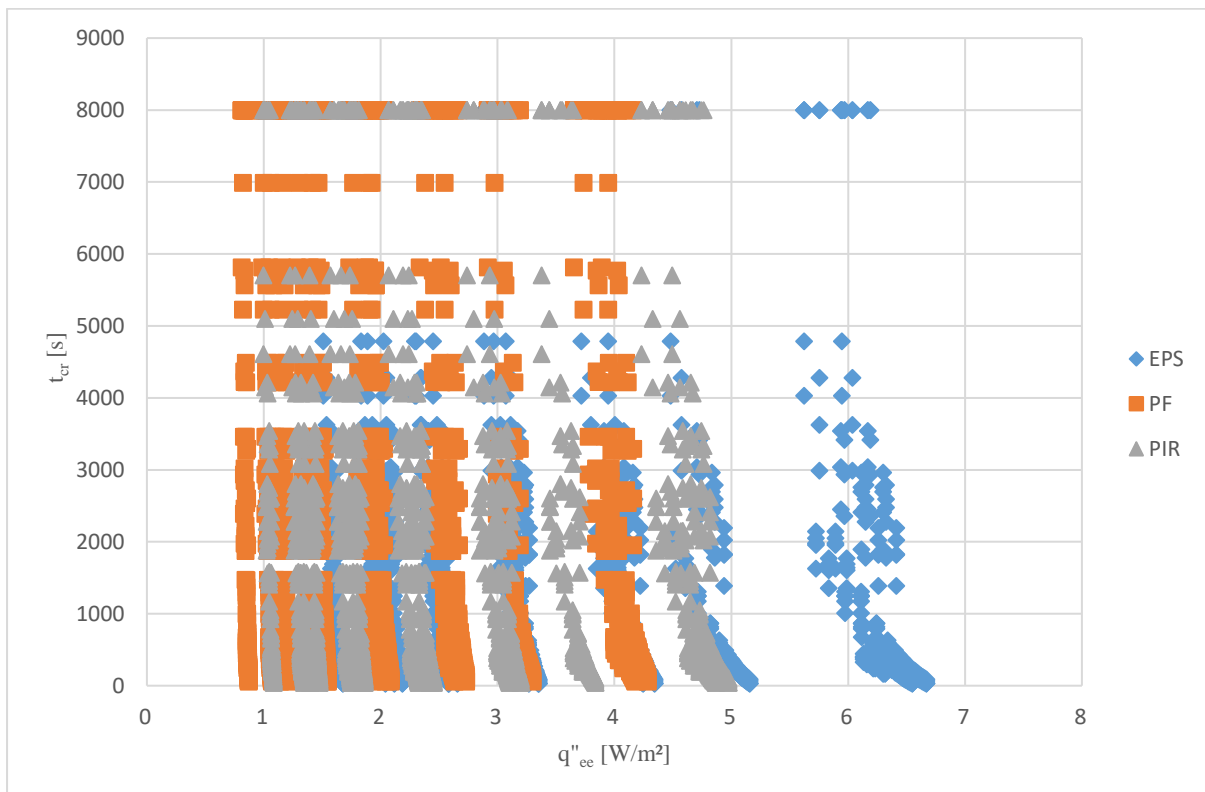

Figure 27: Results for each scenario

33

3.1 Overview of results

As previously stated, assemblies deemed to have acceptable fire safe and energy efficient performance will have a critical time (t_{cr}) higher than the required safe egress time, and a total conduction heat flux ($\dot{q}''_{ee}$) lower than the maximum values provided in Table 1.

Table 8 shows an overview of the minimum thickness of the insulation layer, combined with the thickness of the lining, below which failure would occur from an energy efficiency perspective. It should be noted that not all these cases correspond to the optimum-assembly thickness. As previously stated, the thickness of the first layer (L_1) is equal to the one of the third layer (L_3). In the table, Z stands for climate zone, B for brick and P for plasterboard.

Table 8: Overview of thicknesses below which failure occurs considering energy efficiency performance

[mm]	Z	MgO+EPS	B+EPS	P+EPS	MgO+PIR	B+PIR	P+PIR	MgO+PF	B+PF	P+PF
					Dwelling houses					
L_1	2	3	103	9.5	38	76	9.5	3	65	9.5
L_2		238	188	238	144	144	188	144	144	144
L_1	4	3	103	9.5	38	76	9.5	3	65	9.5
L_2		238	188	238	144	144	188	144	144	144
L_1	7	3	110	9.5	38	90	9.5	3	65	9.5
L_2		238	188	238	144	144	188	144	144	144
					Other buildings					
L_1	2	3	65	9.5	3	110	9.5	no failure	no failure	no failure
L_2		144	144	144	144	92	144			
L_1	4	3	65	9.5	3	110	9.5	no failure	no failure	no failure
L_2		144	144	144	144	92	144			
L_1	7	3	65	9.5	3	65	9.5	no failure	no failure	no failure
L_2		144	144	144	144	144	144			

Table 9 shows an overview of the thickness (in mm) below which a certain assembly would fail from a fire safety point of view. As previously mentioned, only the thickness of the lining material is important in this case. In the table, case 1 indicates a constant heat flux of 30 kW/m^2, case 2 a constant flux of 35 kW/m^2, case 3 the heat flux curve shown in Figure 18, case 4 the standard fire total gauge heat flux shown in Figure 19, and case 5 the heat flux curve shown in Figure 20.

Table 9: Overview of failure thickness when it comes to fire safety below which failure occurs

[mm]	Case	MgO+EPS	B+EPS	P+EPS	MgO+PIR	B+PIR	P+PIR	MgO+PF	B+PF	P+PF
				Dwellinghouses - pre-flashover ($t_{cr} = 120\ s$)						
L_1	1	9	no failure	no failure	7	no failure	no failure	6	no failure	no failure
L_1	2	9	no failure	no failure	8	no failure	no failure	6	no failure	no failure
				Dwellinghouses - post-flashover ($t_{cr} = 120\ s$)						
L_1	3	9	no failure	no failure	8	no failure	no failure	6	no failure	no failure
L_1	4	5	no failure	no failure	4	no failure	no failure	no failure	no failure	no failure
L_1	5	7	no failure	no failure	6	no failure	no failure	4	no failure	no failure
				Other buildings – pre-flashover ($t_{cr} = 400\ s$)						
L_1	1	20	no failure	failure in all	18	no failure	15	14	no failure	12.5

				cases						
L₁	2	20	no failure	failure in all cases	18	no failure	15	15	no failure	12.5
Other buildings – post-flashover ($t_{cr} = 400\ s$)										
L₁	3	24	no failure	failure in all cases	20	no failure	failure in all cases	18	no failure	15
L₁	4	18	no failure	15	15	no failure	15	14	no failure	12.5
L₁	5	20	no failure	16	18	no failure	15	14	no failure	12.5

3.2 Numerical results for assemblies in dwelling houses (low critical time)

Each climate zone will have its own results when it comes to energy efficiency, while from the fire safety point of view, the results previously mentioned are valid for each climate zone, since the temperature differences between indoor and outdoor do not influence the critical time.

3.2.1 Fire safety performance

From a fire safety point of view, when it comes to the two pre-flashover scenarios with constant heat fluxes of 30 and 35 kW/m^2, where the burning item is very close to the assembly, all combinations with brick or plasterboard as lining materials do not reach their critical temperature before 120 s. Failure occurs only when MgO is the lining material:

- when combined with EPS and when the lining thickness is lower than 9 mm for both heat flux scenarios;
- when combined with PIR and the lining thickness is less than 7 mm for a constant heat flux of 30 kW/m^2 and less than 8 mm for a constant heat flux of 35 kW/m^2;
- when combined with PF and the lining thickness is lower than 6 mm for both heat flux cases.

In post-flashover scenarios, failure also occurs only when MgO is the lining material:

- for case 3, failure will occur when the thickness of the MgO is lower than 9 mm when combined with EPS, lower than 8 mm whan combined with PIR, and lower than 6 mm when combined with PF;
- for the standard fire total gauge heat flux curve (case 4), failure only occurs when MgO is combined with EPS, at a thickness lower than 5 mm, and with PIR, at a thickness lower than 4 mm;
- for case 5, failure occurs the thickness of the MgO layer is lower than 7 mm in combination with EPS, 6 mm in combination with PIR, and 4 mm when combined with PF.

In these post-flashover cases, when bricks or plasterboard are used as lining, failure from a fire safety perspective never occurs.

3.2.2 Energy efficiency performance (climate zone 2)

According to the performance criteria set for dwelling houses in zone 2, the optimal results for this case are the ones that have a critical time above 120 s and a total conduction heat flux lower than 2.3589 W/m^2, as shown by the green area in Figure 28.
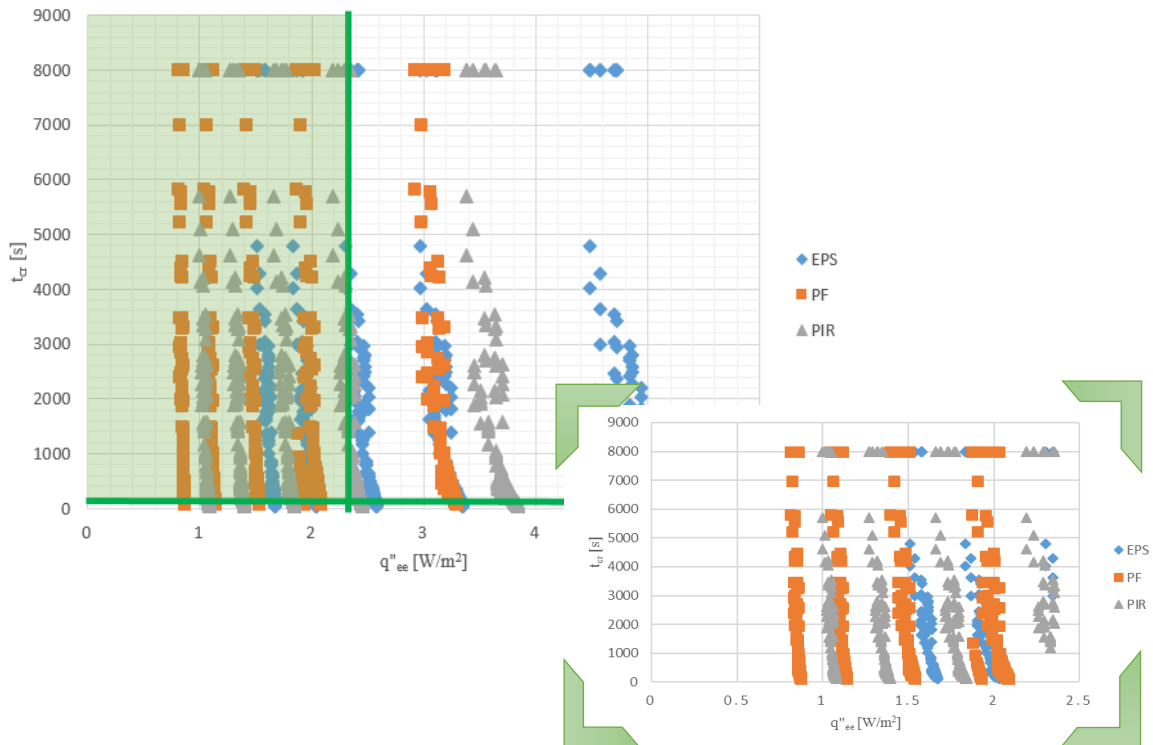

Figure 28: Acceptable results for dwelling houses in climate zone 2

From the obtained results it is possible to see that, from the energy efficiency point of view, the criterion is met:

- when EPS is the insulation material
  - from a thickness of 283 mm when combined with any analysed thickness of MgO or plasterboard;
  - from a thickness of 188 mm when combined with bricks, which should be at least 103 mm thick;
- when PIR is present,
  - from a thickness of 144 mm when combined with MgO or bricks, which should respectively be at least 38 mm and 76 mm thick;
  - from a thickness of 188 mm in any combination with plasterboard;
- in all cases where PF is present, from a thickness of 144 mm.

3.2.3 Energy efficiency performance (climate zone 4)

Optimal results for dwelling houses located in climate zone 4 are the ones with a critical time above 120 s and a total conduction heat flux lower than 2.9842 W/m^2, as shown by the green area in Figure 29.
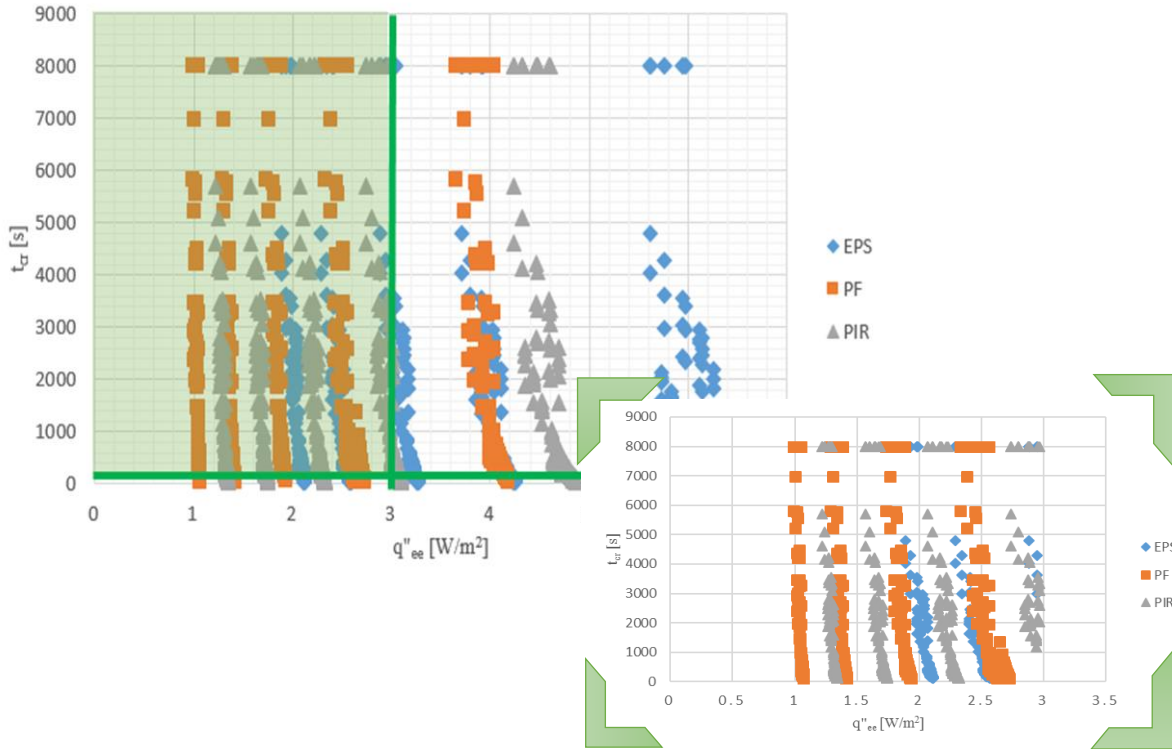
Figure 29: Acceptable results for dwelling houses in climate zone 4

From an energy efficiency point of view, failure occurs in the exact same cases as the ones mentioned in climate zone 2.

3.2.4 Energy efficiency performance (climate zone 7)

Optimal results for dwelling houses located in climate zone 7 are the ones with a critical time above 120 s and a total conduction heat flux lower than 3.0744 W/m^2, as shown by the green area in Figure 30.
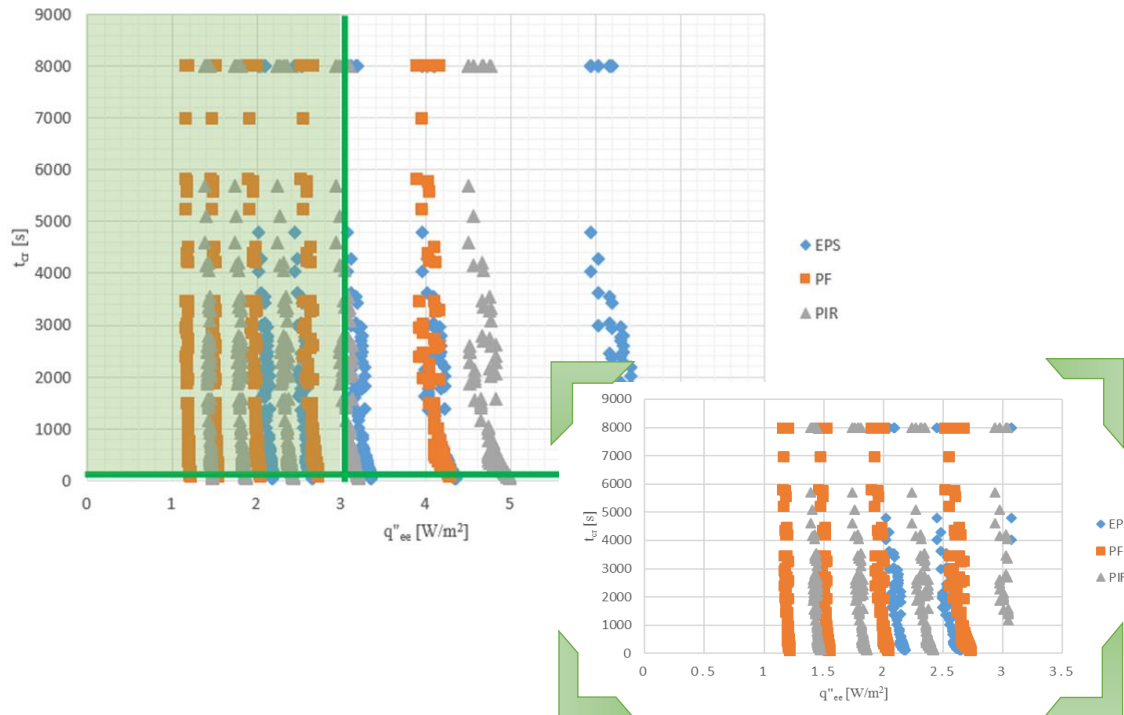
Figure 30: Acceptable results for dwelling houses in climate zone 7

From the obtained results it is possible to see that, from the energy efficiency point of view, the criterion is met:

- when EPS is the insulation material
  - from a thickness of 283 mm when combined with any analysed thickness of MgO or plasterboard;
  - from a thickness of 188 mm when combined with bricks, which should be at least 110 mm thick;
- when PIR is present,
  - from a thickness of 144 mm when combined with MgO or bricks, which should respectively be at least 38 mm and 90 mm thick;
  - from a thickness of 188 mm in any combination with plasterboard;
- in all cases where PF is present, from a thickness of 144 mm.

3.3 Numerical results for assemblies in buildings other than dwelling houses (higher critical time)

For the same type of assembly, the failure from an energy efficiency point of view occurs more often in dwellings houses compared to other types of buildings. This happens because the required U-value for buildings other than dwelling houses is higher compared to the one required for dwelling houses, thus making the value of the performance criteria higher as well.

On the contrary, when it comes to fire safety, failure will happen more frequently, because the performance criteria has a higher value.

3.3.1   Fire safety performance

In the case of pre-flashover fires, where the burning item is very close to the assembly, failure occurs:

- when MgO is the lining material, combined with EPS, PIR or PF, and its thickness is respectively lower than 20 mm and 18 mm for both heat fluxes, lower than 14 mm for a constant heat flux of 30 kW/m^2 and lower than 15 mm for a constant heat flux of 35 kW/m^2;
- in all when plasterboard is combined with EPS. When combined with PIR or PF, failure occurs respectively when the thickness of the lining is less than 15mm and mm 12.5 mm for both heat flux scenarios.

In post-flashover scenarios, fire safety failure occurs:

- for case 3
    - when MgO is the lining material, combined with EPS, PIR, or PF, and its thickness is respectively less than 24 mm, 20 mm, and 18 mm;
    - in all cases where plasterboard is combined with either EPS or PIR, and in when it is combined with PF and its thickness is less than 15 mm;
- for case 4
    - when MgO is the lining material, combined with EPS, PIR, or PF, and its thickness is respectively less than 18 mm, 15 mm, and 14 mm;
    - when plasterboard is the lining material, combined with either EPS or PIR, and its thickness is less than 15 mm, and when it is combined with PF and its thickness is less than 12.5 mm;
- for case 5
    - when MgO is the lining material, combined with EPS, PIR, or PF, and its thickness is respectively less than 20 mm, 18 mm, and 14 mm;
    - when plasterboard is the lining material, combined with either EPS, PIR, or PF, and its thickness is respectively less than 16 mm, 15 mm, and 12.5 mm.

Also in the case of buildings other than dwelling houses, assemblies containing bricks as the lining element will not fail from a fire safety point of view.

3.3.2   Energy efficiency performance (climate zone 2)

Optimal results for dwelling houses located in climate zone 2 are the ones with a critical time above 400 s and a total conduction heat flux lower than 3.4073 W/m^2, as shown by the green area in Figure 31.
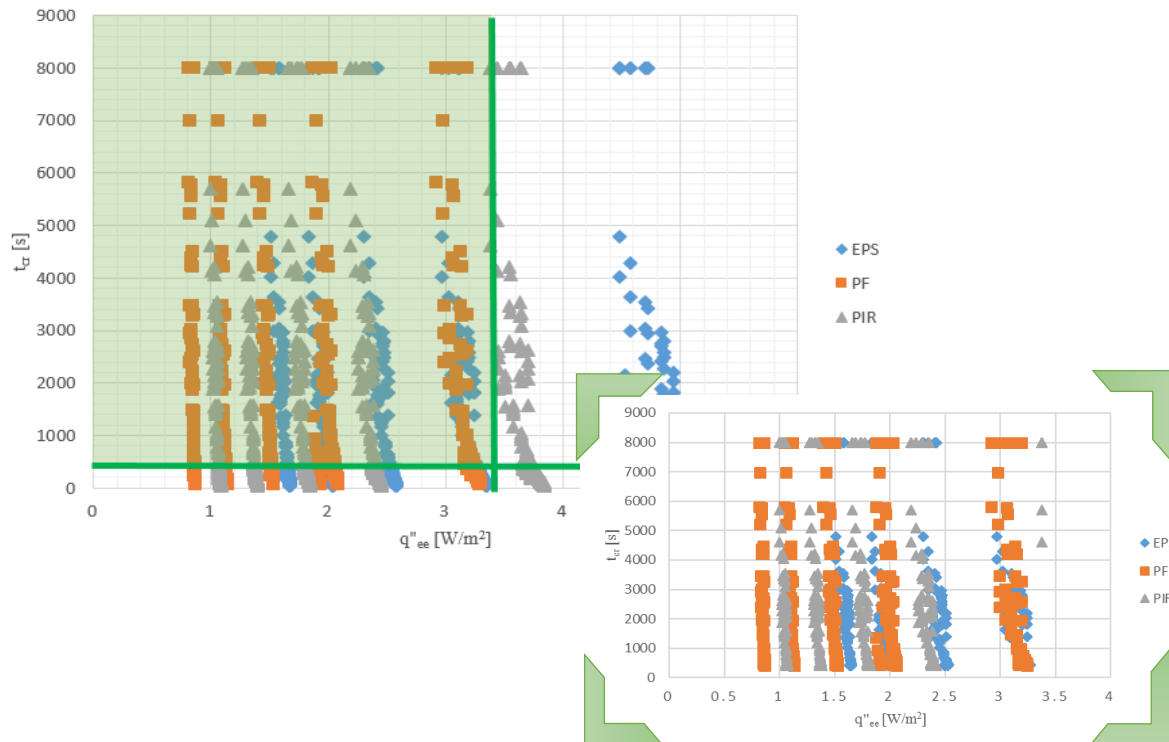
Figure 31: Acceptable results for buildings other than dwelling houses in climate zone 2

From the obtained results it is possible to see that, from the energy efficiency point of view, the criterion is met:

- when EPS is the insulation material with a thickness of at least 144 mm when combined with all types of lining material;
- when PIR is present
  - from a thickness of 144 mm when combined with MgO or plasterboard;
  - from a thickness of 92 mm in combination with bricks, which should be at least 110 mm thick;
- in all cases where PF is present.

3.3.3 Energy efficiency performance (climate zone 4)

Optimal results for dwelling houses located in climate zone 4 are the ones with a critical time above 400 s and a total conduction heat flux lower than 4.3105 W/m², as shown by the green area in Figure 32.
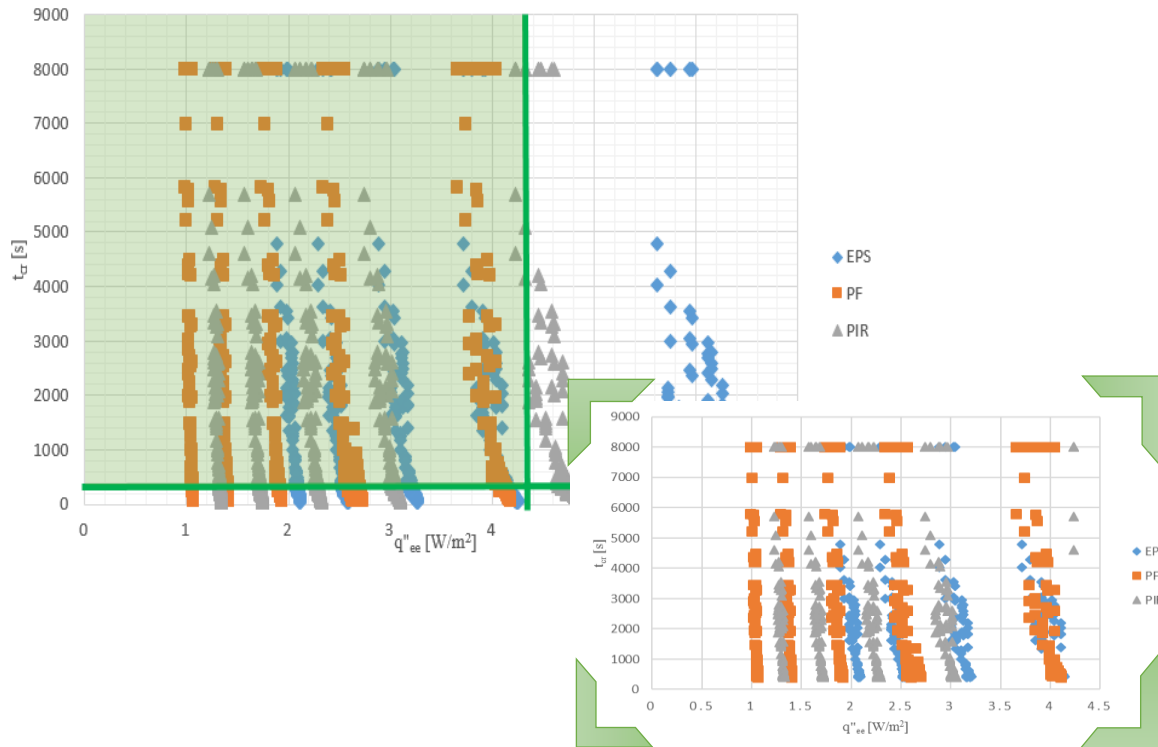
Figure 32: Acceptable results for buildings other than dwelling houses in climate zone 4

From the obtained results it is possible to see that, from the energy efficiency point of view, the criterion is met for the same cases as in climate zone 2.

3.3.4 Energy efficiency performance (climate zone 7)

Optimal results for dwelling houses located in climate zone 7 are the ones with a critical time above 400 s and a total conduction heat flux lower than 4.4408 W/m^2, as shown by the green area in Figure 33.
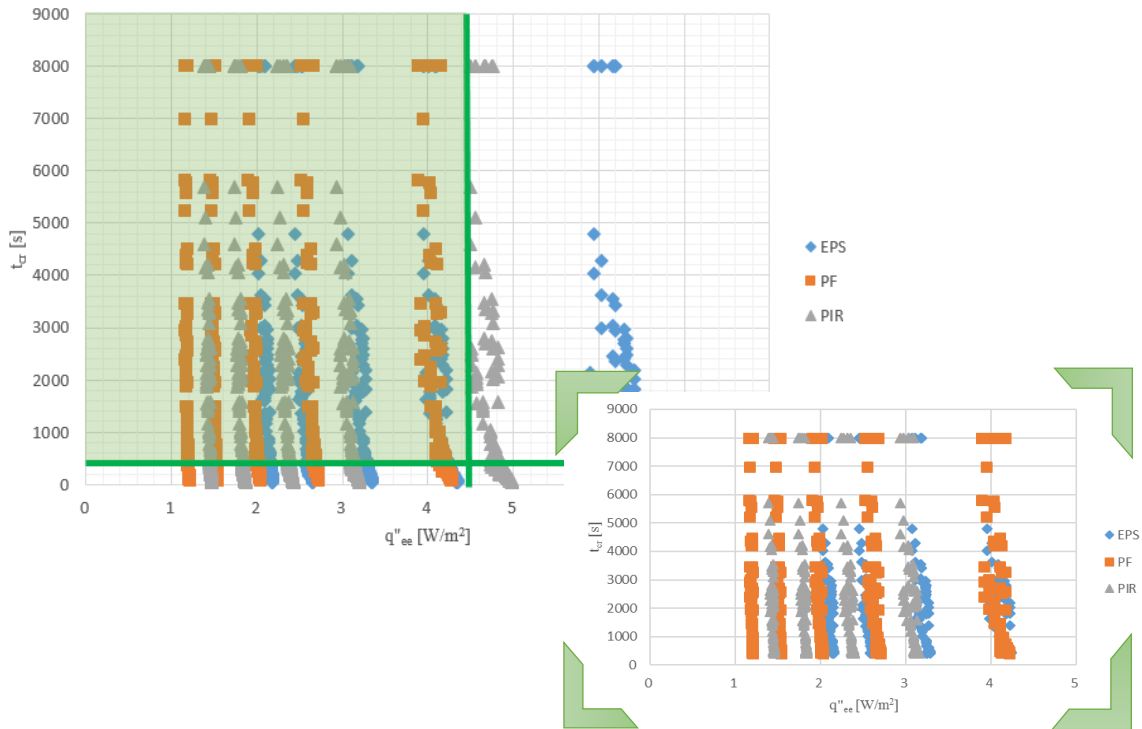
Figure 33: Acceptable results for buildings other than dwelling houses in climate zone 7

From the obtained results it is possible to see that, from the energy efficiency point of view, the criterion is met in all cases where PF is the insulation material, and when either EPS or PIR are present and their thickness is at least 144 mm.

3.4 Experimental results for fire safety validation

Results from the test performed on the SIP were acquired with a camera which recorded the experiment, as well as with the thermocouples inserted from the back of the panel.

Since MgO is a non-combustible material, ignition did not occur, however, the lining material cracked once the radiant panel was turned off and the sample started to cool down, thus losing its integrity.

The highest temperature inside the panel was recorded by thermocouple 5015, at 405°C. The thermocouple was located 164 mm deep, inside the MgO layer; this can be seen in Figure 37.

The highest temperature reached by the EPS is 268°C, measured by thermocouple 1025 placed 153 mm deep; this can be seen in Figure 36.

It is possible to see from the plateau that happens at about 90-100°C that the EPS shrinks after only a few minutes from the start of the test. Thermocouples originally placed within the EPS layer are now able to read gas-phase temperatures, as indicated by the noisy reading given by the thermocouples. When EPS melted onto the thermocouples it made an artificial reading, as can be seen from solid line after the noisy readings.

From Figure 34 it is possible to see that the temperatures in the upper right corner never reach 300°C.
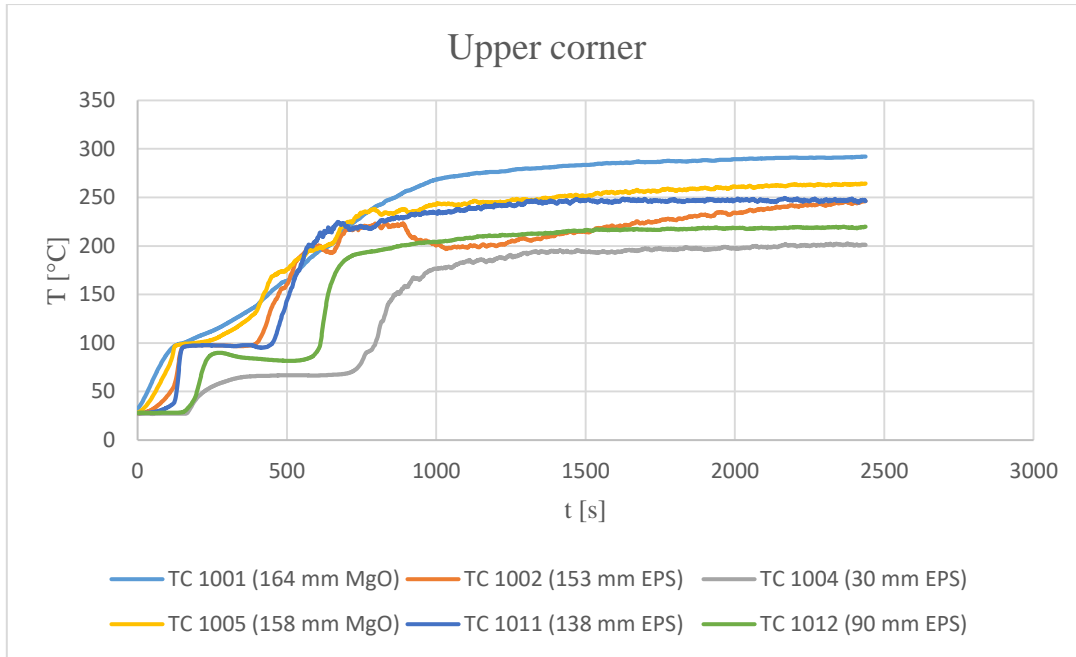
42

Figure 34: Temperature measurements inside the right upper corner of the panel

In Figure 35 it is possible to see the temperatures reached by the MgO and EPS in the centre-right side of the panel (when looking from the back of the sample). The noisy reading of the thermocouples indicates that EPS has shrunk, and consequently the thermocouples are measuring the temperature of the air within the assembly in the space created by the shrinkage of the EPS.
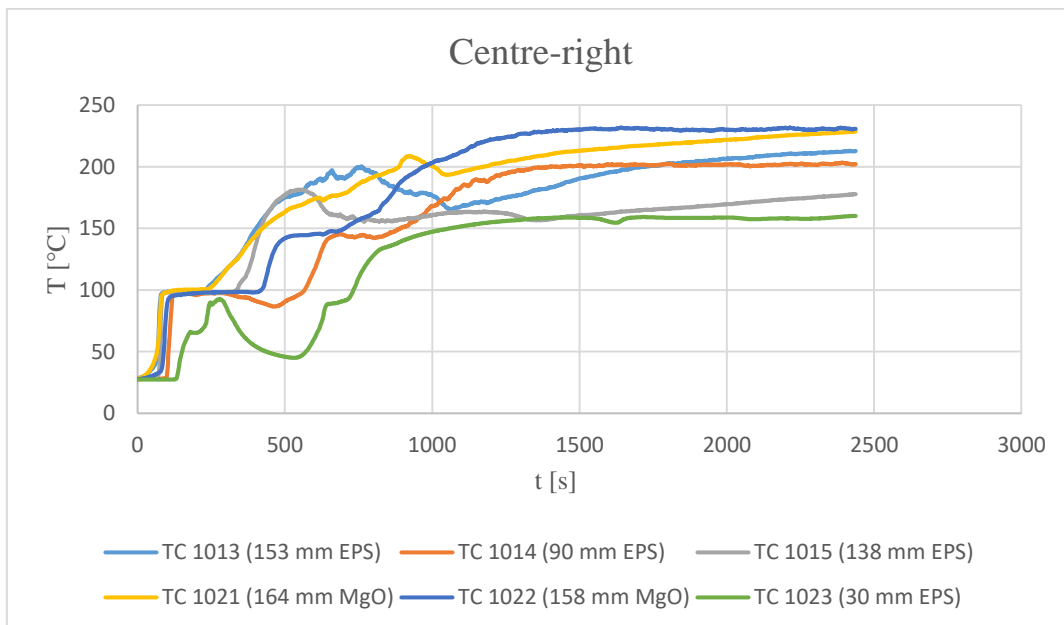

Figure 35: Temperature measurements inside the centre-right of the panel

The highest temperatures inside the EPS were measured in the centre of the sample's EPS layer, as can be seen in Figure 36.
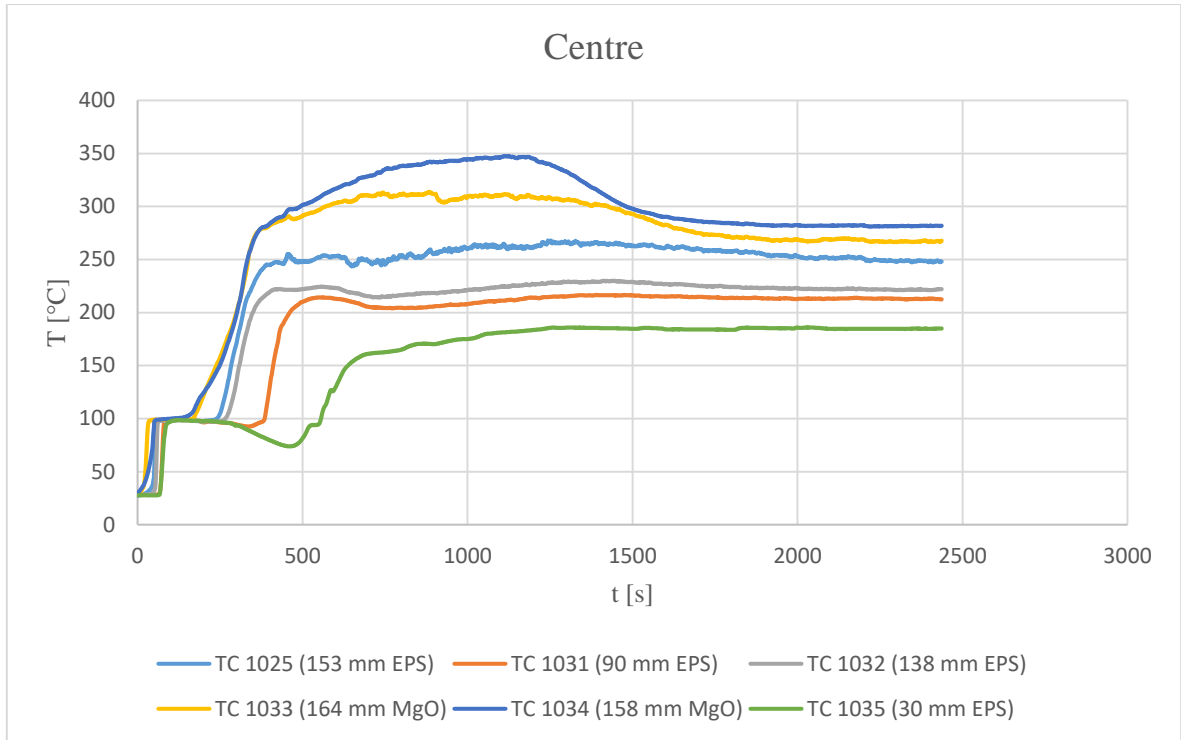
43

Figure 36: Temperature measurements inside the centre of the panel

Figure 37 shows the variation of temperature over time in the centre-left side of the panel. Here is where the MgO reaches its maximum temperature.
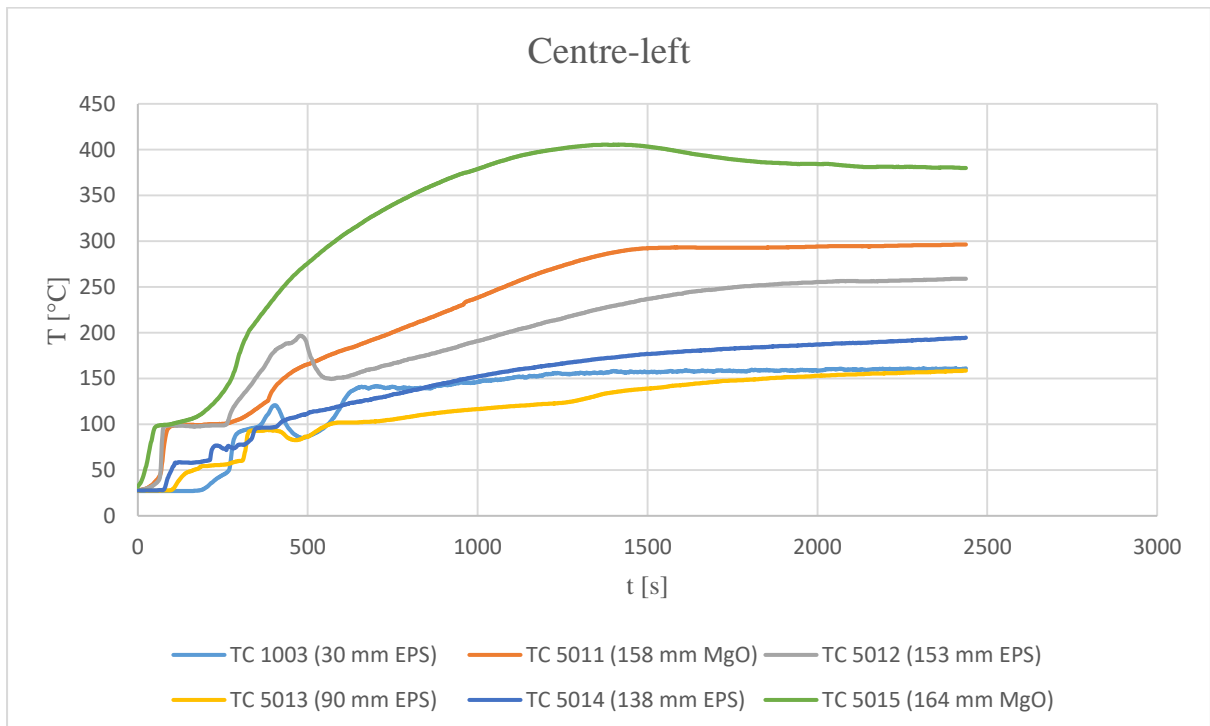

Figure 37: Temperature measurements inside the centre-left side of the panel

From Figure 38 it can be seen that the bottom part of the sample is the one with the lowest temperatures, which barely reach 140°C in the EPS layer. The lack of noisy reading means that the EPS has not shrunken considerably reached its gas phase.
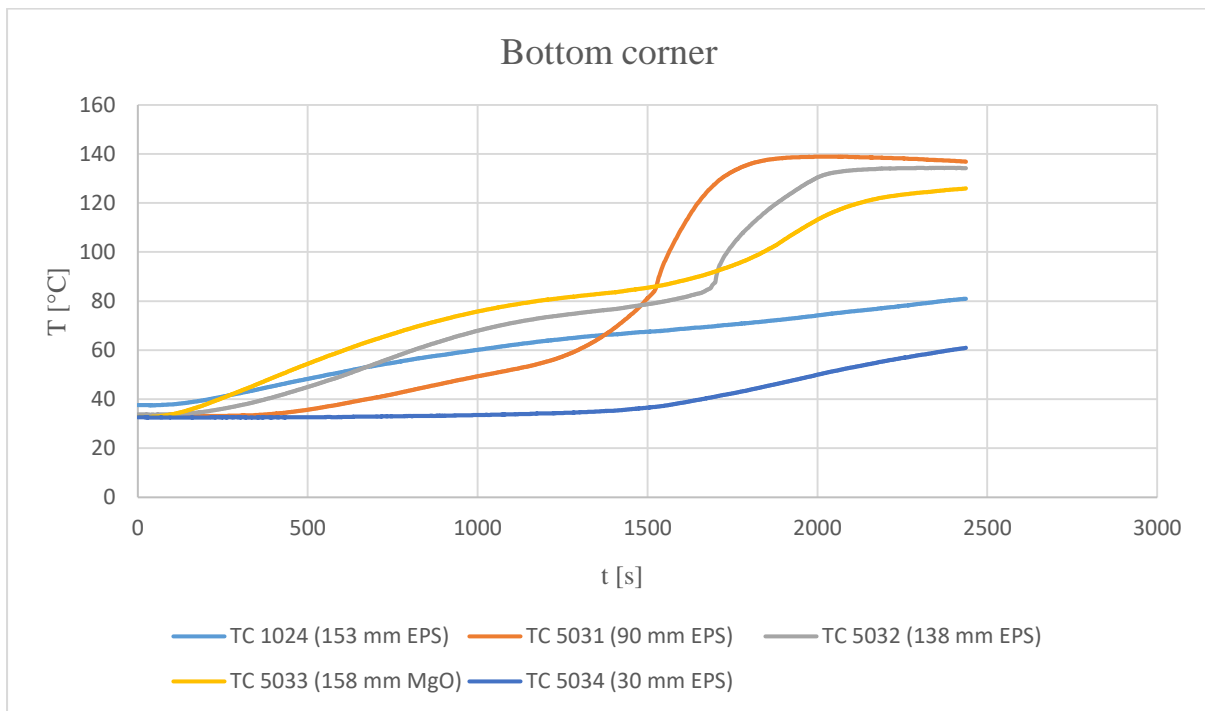

Figure 38: Temperature measurements inside the bottom right corner of the panel

Figure 39 and Figure 40 show, and confirm, that the EPS shrunk and melted completely, apart from the bottom part, where it remained unaltered.

Figure 39: Inside of sample after the test

As shown in Figure 40, the EPS shrunk and melted, going from a thickness of 144 mm to a thickness of approximately 20-25 mm. The bottom part maintained however a thickness of 144 mm.

Figure 40: Measurement of EPS in the bottom part of the sample after the test

This experiment shows the complex behaviour of EPS, which shrunk and melted in some locations, but never reached ignition. The shrinking behaviour helped to delay or avoid this process, however the system lost integrity and produced hazardous molten EPS.

4 Discussion

4.1 Overall discussion of the obtained results

Assemblies deemed to provide an acceptable fire safety and energy efficiency performance should comply with the performance criteria set for both conditions. When it comes to analysing assemblies in dwelling houses (smaller critical time case), the performance criterion to which the results are compared to is stricter from the energy efficiency point of view than the fire safety one. The opposite happens for buildings other than dwelling houses (larger critical time), where the required safe egress time is longer.

As can be seen from the obtained results, even when an insulation material is encapsulated, the hazard created by the onset of pyrolysis still exists. Also, the presence of insulation materials does not make an assembly energy efficient per se, as can be seen from the graphs presented in the previous chapter.

It can be noticed that the thickness of the insulation material is the most important variable from the energy efficiency point of view, while from a fire safety perspective the most important variable is the thickness of the lining material, along with the thermo-physical properties of both the lining and insulation materials. This situation sets a conflictive scenario when trying to optimise an assembly system.

A trend that can be seen when looking at the total conduction heat flow is that its lowest obtained values are those for climate zone 2, while the highest values are those for climate zone 7. The reason for this that the monthly temperature variations in zone 7 are much higher when compared with those in the other two analysed zones.

When looking at the overall picture of all the obtained results, those which are both fire safe as well as energy efficient, and are thus acceptable results, are only 4044/7200 (about 56%) for dwelling houses (lower critical time), and 3261/7200 (about 45%) for buildings other than dwelling houses (larger critical time).

4.1.1 Noticeable material performance

From the results in Table 8 and Table 9 it can be seen that when PF is the insulation material, the thicknesses needed for both layers of an assembly which is both fire safe and energy efficient are lower compared to the other insulation materials. Out of the three analysed combustible insulation materials, PF has the highest thermal inertia, but lowest thermal conductivity. When it comes to energy efficiency, the lower the thermal conductivity, the lower the steady-state and cyclic transmittances, thus the lower the total conduction heat flux for the same climate zone. From a fire safety perspective, PF has a higher critical temperature compared to the other two materials, making it possible to have lower thicknesses for the lining material.

When bricks are used as lining material, there is no failure of the assembly from a fire safety perspective, as indicated by the green area in Figure 41. This happens because bricks have a high thermal inertia, so consequently, according to the heat transfer model, the critical time will be higher as well. However, as previously stated, when looking at the energy efficiency, the lining material is not as significant as for fire safety, thus failure from this point of view

will occur even when brick is the encapsulation material. This is why the total thickness of an assembly is an important factor.
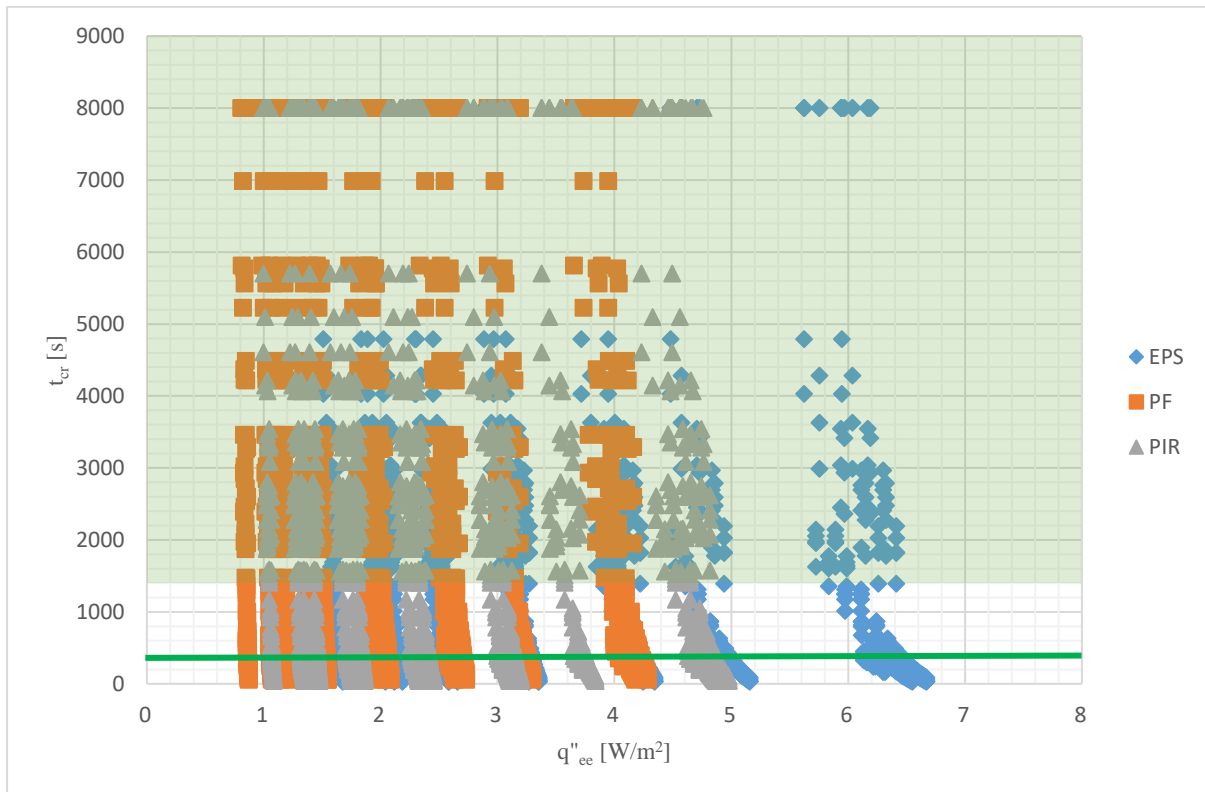

Figure 41: Indication of the area (in green) where the results of assemblies with brick lining are located

From Table 9 it is noticeable that when it comes to fire safety, in many scenarios where the lining material is plasterboard, failure happens for all thicknesses of the material.

4.1.2 Non-dominated results

Within the results obtained in the case of assemblies present in dwelling houses, as well as in the case of buildings other than dwelling houses, there will be non-dominated results for each analysed climate zone. Non-dominated results lie at the limits of the acceptable results area, and are characterised by the fact that there is no other feasible solution which can be better without worsening one of the set criteria [67]. These are not optimal results, but they are however efficient. Non-dominated solutions are useful to find the Pareto frontier. This however, is not the purpose of this thesis,

An example of non-dominated results can be seen in Figure 42, where the red circle indicates the area where a non-dominated result can be found.
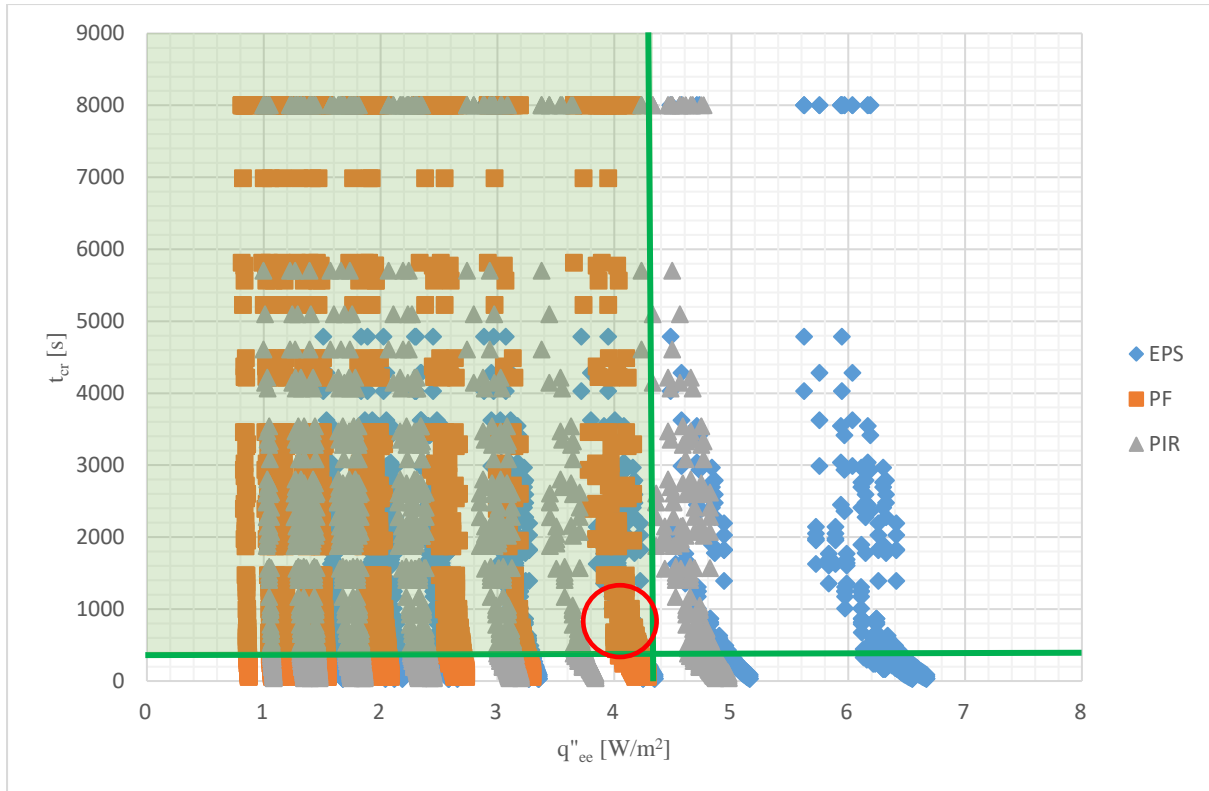
Figure 42: Non-dominated results for buildings other than dwelling houses in climate zone 4

4.2 Comparison with experimental results

Results obtained from the heat transfer model presented in section 2.2.1 are compared to those obtained from experimental tests found in the literature, as well as personally performed, in order to validate the model itself.

4.2.1 SIP sample

The properties of the sample described in section 2.5.2 are assumed to be those indicated in Table 3 and Table 4. This assumption is made because not all exact thermo-physical properties of the sample were presented. As shown in Figure 22, the thickness of the MgO layer is 12 mm, while the thickness of the EPS layer is 144 mm. The sample was exposed to a constant heat flux of 65 kW/m^2 for a period of about 40 minutes. All these values are used as inputs for the heat transfer model, which gives as output a critical time of 137 s for a critical temperature of 240 °C. It is important to notice that, when modelling the performed test, the critical temperature is assumed to be equal to the melting temperature of the material.

When looking at the temperature data collected by the thermocouples at that same time, it can be seen that both MgO and EPS have barely reached 100°C. At that temperature the EPS has started to shrink, as can be seen from the plateau in Figure 34 to Figure 37.

In the upper corner, melting temperatures (240 °C) are first reached at a depth of 138 mm about 18 minutes into the experiment (indicated by the blue line), while at the same time temperatures at a depth of 153 mm (thus closer to the radiant panels) are much lower, as can be seen in Figure 43: Temperature measurements inside the EPS in right upper corner of the

Figure 43. This is explained by the fact that the EPS has shrunk, and thus there is a gap between the insulation material and the MgO, where air is present, as confirmed by the noisy temperature readings.
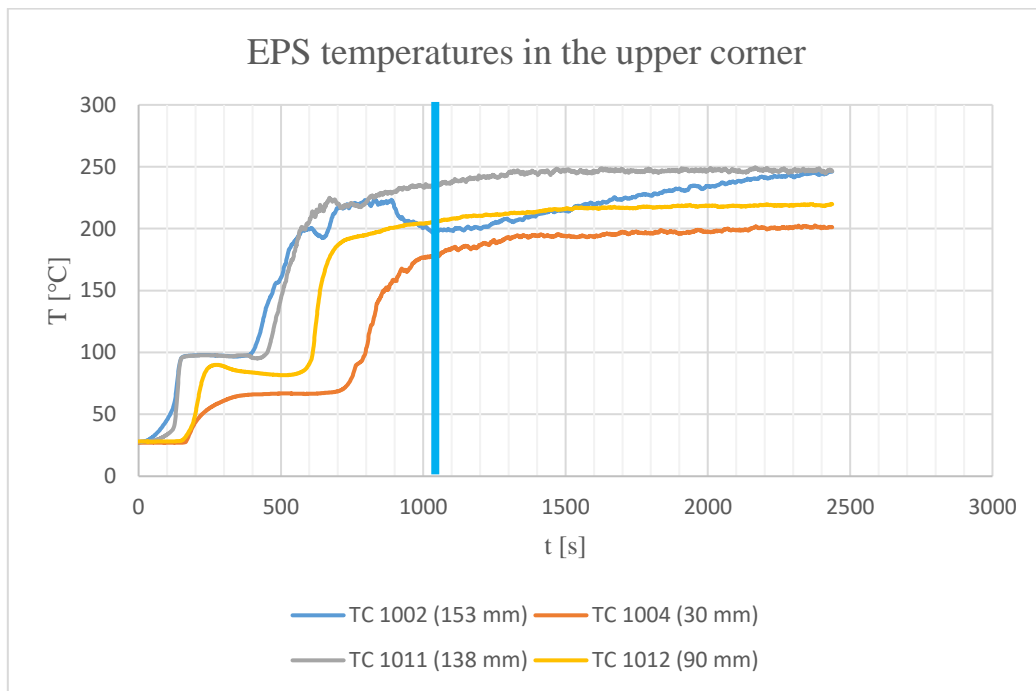

Figure 43: Temperature measurements inside the EPS in right upper corner of the sample

In the centre-right of the sample, thermocouple data indicates that the melting temperature is never reached, as can be seen from Figure 44. However, when opening the sample after the test, it was possible to see that also in that part of the sample melting had occurred.
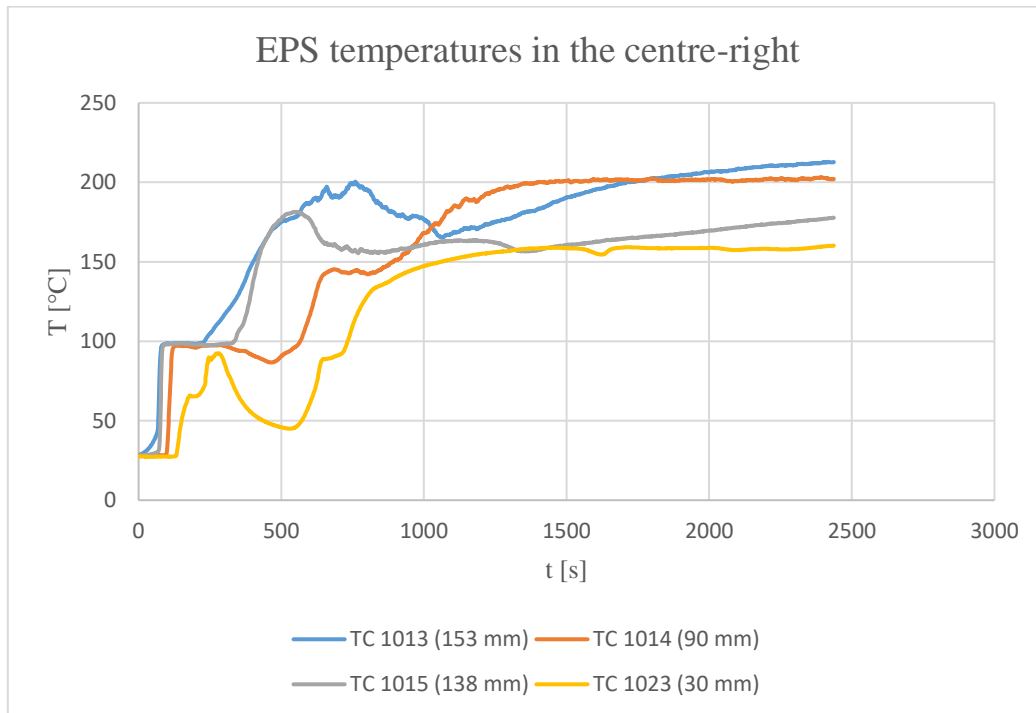

Figure 44: Temperature measurements inside the EPS in the centre-right of the sample

In the centre of the sample, right in front of the radiant panel, temperatures reached 240°C at 153 mm at a time of 6.25 min, while temperatures at lower depths never reach that value, as indicated by the blue line in Figure 45. The same behaviour is noticeable in the centre-left side of the sample, with the difference that the critical temperature is reached at 26 min, as indicated by the blue line in Figure 46.
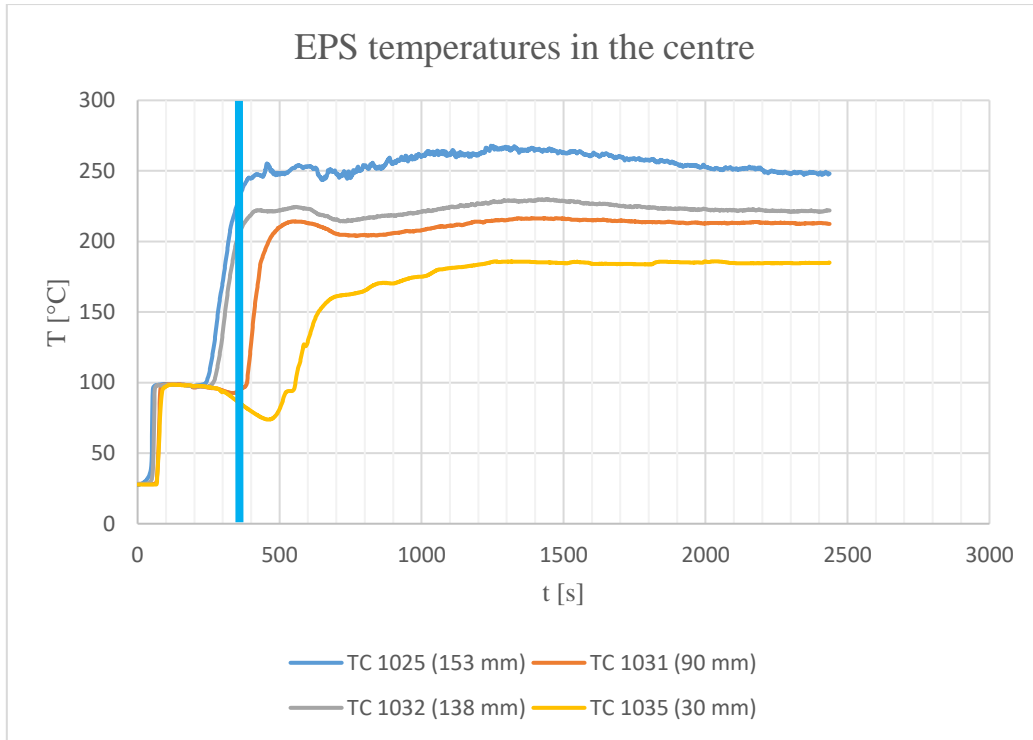

Figure 45: Temperature measurements inside the EPS in the centre of the sample
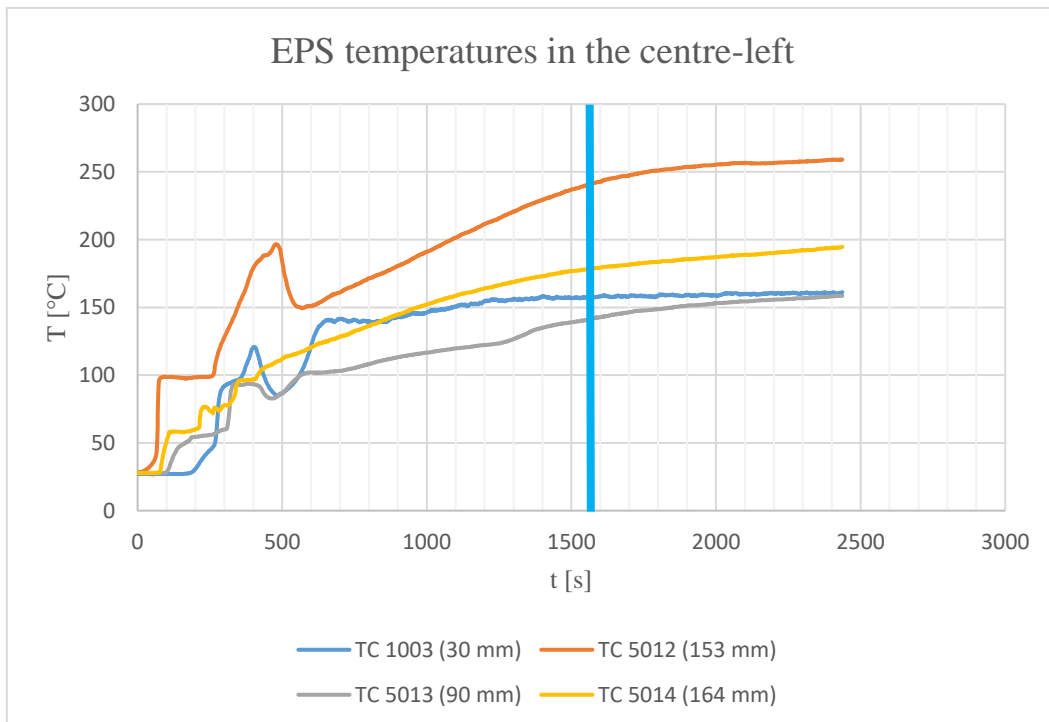

Figure 46: Temperature measurements inside the EPS in the centre-left of the sample

The bottom of the sample reaches shrinking temperatures only in the upper part, where, as can be seen from Figure 39, some shrinking occurs. However, at the very bottom of the sample, no shrinking occurs since temperatures barely reach 80°C, as can be seen from Figure 38. In the whole bottom part of the sample, critical temperatures are never reach, so no melting occurred.

From visual observation it was possible to see that the EPS did not ignite, and integrity of the sample was kept until the sample itself started to cool down.

4.2.2   Comparison with results found in the literature

4.2.2.1   Plasterboard and PIR

Hidalgo et al. tested a system containing plasterboard as lining material (12.5 mm thick) and PIR as insulation (100 mm thick) exposed to a radiative heat flux of 65 kW/m^2 [68]. After 1 min from the start of the test the plasterboard's exterior render was consumed, and a significant amount of vapours were released from the material during the first 5 min. Release of volatiles through the plasterboard frame edges was observed after 17 min, which is consistent with the interface achieving the critical temperature of 300°C at 16 min [68].

When applying the methodology explained in section 2.2.1, with the same inputs as the experiment and the thermos-physical characteristics given in Table 3 and Table 4, the obtained critical time is 250 s.

4.2.2.2   Plasterboard and PF

A system containing plasterboard as lining material (12.5 mm thick) and PF as insulation (100 mm thick) was exposed to a radiative heat flux of 65 kW/m^2. The critical temperature was achieved at the interface after 21 min [68].

When applying the methodology explained in Paragraph 2.2.1, with the same inputs as the experiment and the thermos-physical characteristics given in Table 3 and Table 4, the obtained critical time is 337 s.

4.2.3   Overall discussion

Table 10 shows the critical time of three different types of assemblies obtained experimentally and with the heat transfer model.

Table 10: Comparison between experimental and modelled critical time

Assembly	$t_{cr,experimental}$ [s]	$t_{cr,model}$ [s]
MgO + EPS	375	137
Plasterboard + PIR	960	250
Plasterboard + PF	1260	337

The results obtained from the test performed on a SIP with MgO as lining material and EPS as insulation confirm that the methodology used to find the critical time is not suitable for materials with shrinking and melting behaviour, such as EPS. This because the critical temperature used in the methodology is actually the melting temperature, and not the shrinking one, which is actually lower, as shown by the experimental results in section 4.2.1. Also, the methodology utilised does not take into account the fact that a gap will form between the lining material and the insulation, due to its shrinking behaviour. The shrinking

will create issues when it comes to the integrity of the assembly, and allow for smoke and mixing of pyrolysis gases and air.

In all cases, the critical time obtained by applying the heat transfer model is very conservative. When plasterboard is the lining material, a justification for this is that the heat transfer model does not account for the endothermic reaction which takes place within the material [68].

Also, one of the assumptions of the model is that convective heat losses are assumed to be negligible. When including convective losses with a coefficient of losses $h_c = 10 \, W/m^2 K$, the critical time goes from 137 s to 144 s in the case of MgO-EPS, 250 s to 263 s in the case of plasterboard-PIR, and from 337 s to 359 s in the case of plasterboard-PF. This is proof that the assumption previously mentioned is valid, and this is not the main source of uncertainty, but the assumption of inert behaviour from the lining is.

4.3 Comparison with assemblies containing non-combustible insulation

Assemblies containing non-combustible insulation, such as stone wool, are 100% fire safe, and are thus an optimal solution from a fire safety point of view. In order to see if these types of assemblies are also optimal from an energy efficiency perspective, a comparison is made between assemblies containing non-combustible materials and assemblies containing combustible insulation. Table 11 shows the properties of stone wool, material used as an example of non-combustible insulation.

Table 11: Thermo-physical properties of stone wool [37]

Thermal conductivity k [W/mK]	Density ρ [kg/m^3]	Specific heat capacity c [J/kgK]
0.044	40	840

Figure 47 and Figure 48 show the comparison between assemblies containing combustible and non-combustible insulation for dwelling houses in climate zone 2. The red line indicates the maximum $\dot{q}''_{ee}$ value after which the assembly's energy efficiency performance is deemed unacceptable.
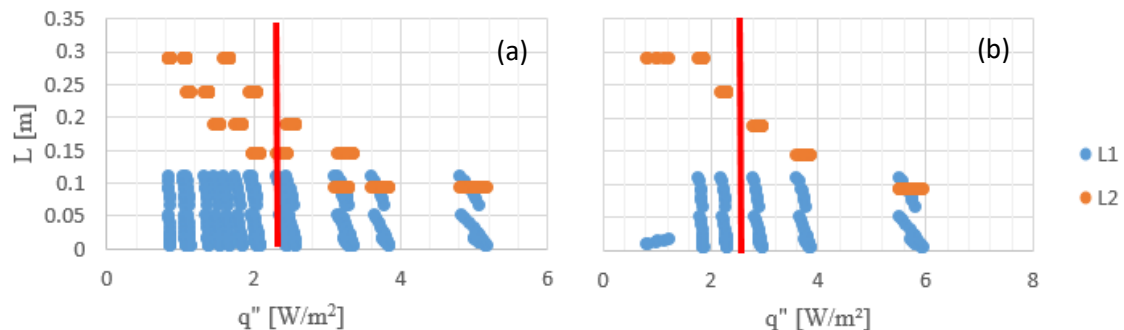

Figure 47: Total conduction heat flow depending on the thickness of lining and insulation layers for (a) combustible insulation and (b) non-combustible insulation
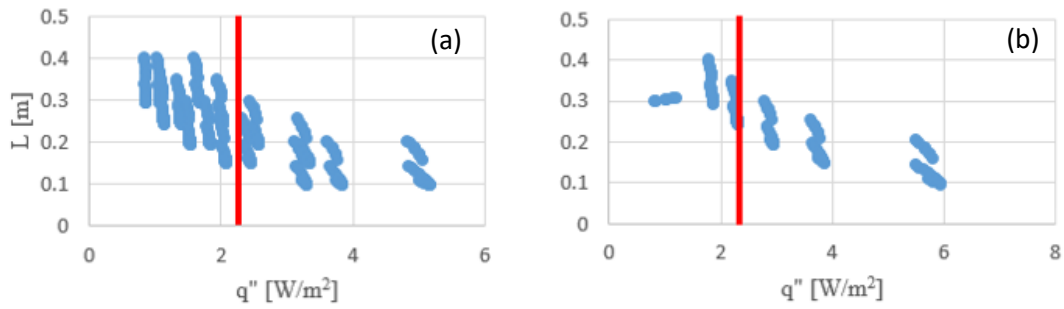
Figure 48: Total conduction heat flow depending on the total thickness of an assembly for (a) combustible insulation and (b) non–combustible insulation

It is noticeable that when combustible insulation is present, assemblies can be about 10% thinner, and still comply with the energy efficiency criterion. The same conclusion can be made for all climate zones as well as for buildings other than dwelling houses.

4.4 Metal faced sandwich panels

Metal faced sandwich panels have a non-combustible lining and are considered optimal when it comes to insulation. However, standard thicknesses of the lining are very thin (usually below 1 mm [69]), allowing the thermal wave to reach the insulation material quickly.

A sandwich panel where steel is the lining material, with a thickness of 1 mm, and EPS is the insulation material, with a thickness of 289 mm, is considered. The properties of steel can be found in Table 12, while those of EPS can be found in Table 3.

Table 12: Properties of stainless steel

Thermal conductivity k [W/mK]	Density ρ [kg/m³]	Specific heat capacity c [J/kgK]
16[58]	8000[70]	500[71]

When looking at a sandwich panel exposed to a constant heat flux of 30 kW/m², the critical time obtained from the heat transfer model is 38 s. When the heat flux is 65kW/m², the critical time becomes 18 s. These times, even though they are conservative, are very small compared to the required safe egress time, as well as the previously studied cases. From the energy efficiency point of view, however, optimal solutions can be achieved, as shown in Table 13.

Table 13: Comparison of the total conduction heat flow through a metal faced sandwich panel with the performance criteria set for each climate zone

Zone	$\dot{q}^{"}_{panel}$ [W/m²]	$\dot{q}^{"}_{max}$ [W/m²] - Dwellings	$\dot{q}^{"}_{max}$ [W/m²] – Other than dwellings
2	1.6800	2.3589	3.4073
4	2.1240	2.9842	4.3105
7	2.1910	3.0744	4.4408

Consequently, metal faced sandwich panels are ideal assemblies from an energy efficiency perspective, as well as thickness, but do not comply at all with the fire safety criterion.

4.5 Uncertainties

4.5.1 Methodology uncertainties
Both models have the same uncertainty given by the thermal contact resistance caused by the limited contact area between different materials in an assembly. When a junction is formed by pressing two similar or dissimilar materials together, only a small fraction of the nominal surface area is actually in contact because of the non-flatness and roughness of the contacting surfaces [72]. This restricts the heat transfer from one material to another. Both the energy efficiency and the fire safety models do not take into account the thermal contact resistance, making the two proposed models to be conservative.

Different uncertainties for both utilised models are presented in the following sections.

4.5.1.1 Fire safety methodology
A great uncertainty in the heat transfer model is given by the boundary conditions to which the assembly is exposed to. There are infinite possible fire scenarios, which depend on variables such as the compartment's dimensions, the ventilation conditions, the fuel load present in the compartment, and the position of the fire inside the compartment. These are all variables that cannot be predicted with certainty, unless a more extended analysis is performed.

Assumptions have been made when it comes to the emissivity and absorptivity values, as well as for the heat transfer coefficient of losses. When it comes to the latter, convective heat losses have been neglected, with the assumption that in the case of a single burning item, as well as in post-flashover fires, radiative losses are much greater than the convective ones. This however, does not influence obtained results greatly, as explained in section 4.2.3.

The values of thermal conductivity, density, and specific heat capacity can vary, since a range of values exits for each property of each material. In addition, those values may change when the temperature changes, while in the model they will have the same value even when the temperature increases.

Hidalgo performed an inverse analysis to find the real conductivity of PIR and PF. When assuming that density and specific heat capacity do not change with temperature, values found for thermal conductivity were larger than those stated at ambient temperature [8]. Higher thermal conductivity values give higher critical time values. This becomes thus an uncertainty in the methodology, which causes the model to be conservative.

As previously stated, the model does not take into account endothermic reactions, such as the one that takes place within plasterboard when it is exposed to a heat flux. The fact that these reactions are not taken into account makes room for uncertainties in the heat transfer model, since endothermic reactions might delay the progression of the thermal wave.

The calculation for the surface resistance (R-value), along with the one for the thermal transmittance (U-value) is assumed to be independent of surface roughness [49]. This creates some uncertainties, since the surface roughness could influence the thickness of the assembly.

Another uncertainty is given by the fact that the calculation of the U-value assumes that the direction of the heat flow is perpendicular to the plane of the structure. This might not happen in many cases, since the assumption is true when layers are of uniform thickness and the thermal conductivity is isotropic along the plane [49]. However, this a minor uncertainty in the analysed cases, because comparisons are made between assemblies with same thicknesses, assuming isotropic thermal conductivity.

Uncertainties are also created because of the assumption that there is no variation in the spatial distribution of air temperature [49].

4.5.2   Experimental uncertainties

Uncertainties present in the results obtained from experimental testing include the heat exposure to the sample, which may not be uniform throughout the surface of whole sample, but may be sections of the surface where the heat flux onto the sample has lower values.

The exact depth at which thermocouples those are placed is also uncertain, and may vary a few mm compared to the depths stated in Table 7.

Another uncertainty is given by the shrinking and melting behaviour of EPS. It is not clear from the temperature data collected by the thermocouples to see where and exactly at what instant the EPS starts to shrink and melt. The locations of the shrinking and melting can only be seen when the test is concluded and the sample can be analysed visually.

5   Conclusions

Assemblies containing combustible insulation materials can be both fire safe and energy efficient depending on the climate zone in which they are used, and the required safe egress time of the building typology. A framework, which could be of utility to manufacturers and designers, is proposed in order to design assembly types which present a quantifiable and deemed acceptable fire safety and energy efficiency. This framework is shown in Figure 49, and provides the steps needed for the design. These steps consist in assessing the performance criteria for both principles, utilising the proposed methodologies in order to obtain quantitative results, and selecting the necessary input parameters (i.e. type of assembly, fire scenarios, climate zone, etc.).
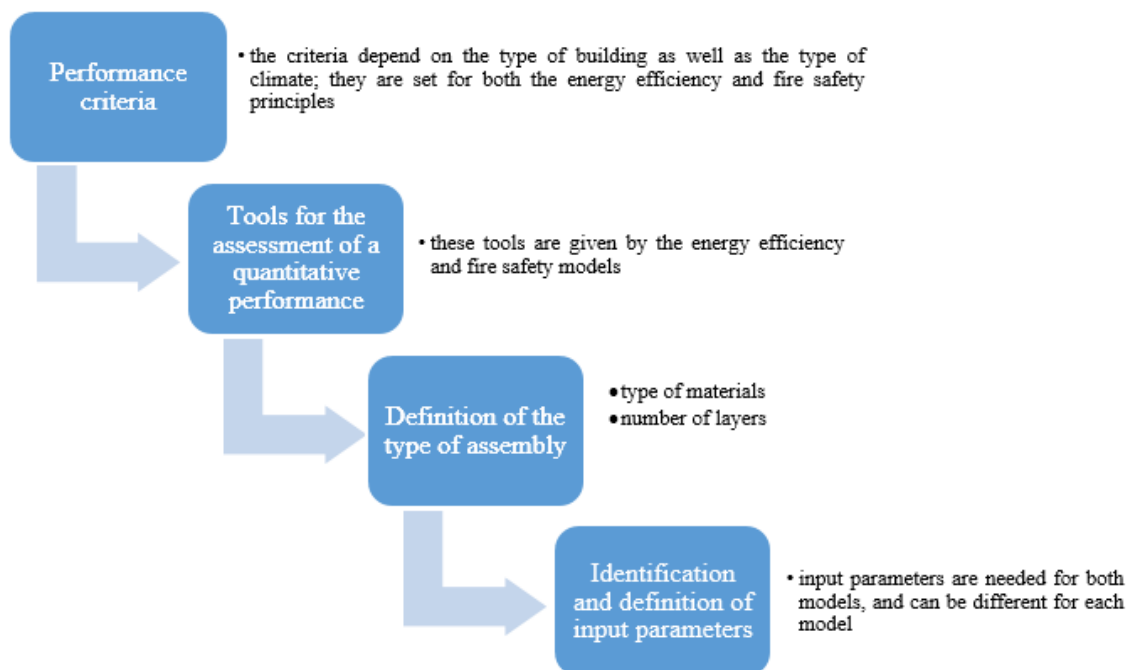

Figure 49: General framework

If the performance criteria are not met from the energy efficiency perspective, the thickness of the insulation material should be increased, while if they are not met from the fire safety point of view, either the thickness of the lining material should be increased, or materials with higher thermal inertia should be utilised.

The methodology presented is conservative from a fire safety perspective, as can be seen when comparing obtained results with experimental ones. The same can be said for the energy efficiency methodology. However, even if conservative, the two methodologies give valuable indications to practitioners on how to address the multi-criteria problem.

From the analysed scenarios, it is possible to conclude that PF is a better combustible insulation material, in comparison with EPS and PIR, from both the fire safety and energy efficiency perspective. This material allows also for thinner assemblies, with total thickness such as 106 mm (14 mm MgO and 92 mm PF) for buildings other than dwellings and 147 mm (3 mm MgO + 144 mm PF) for dwellings.

Even when the lining material is non-combustible, and the assembly is ideal from the energy efficiency perspective, failure from a fire safety point of view can happen. Examples of this are SIPs containing MgO, as well as metal faced sandwich panels. However, when bricks are the lining materials, failure will never happen from a fire safety perspective, while it might happen from an energy efficiency point of view.

From the obtained results it is also possible to conclude that, when combining the two criteria of fire safety and energy efficiency, the use of combustible insulation is slightly more advantageous compared to the use of non-combustible insulation, because it allows for thinner assemblies (about 10% thinner), thus reducing the space needed for these construction systems.

The approach presented to find optimal results for assemblies from both an energy efficiency and fire safety point of view does not yet include a cost analysis. It can be assumed that the thinner the assembly, the less the cost will be. Future work should focus on cost-analysis, as well as on finding a Pareto frontier, which yields all potentially optimal solutions. Additionally, it should also consist in the validation of the energy efficiency model.

Acknowledgements

References

[1] United Nations, United Nations Environment Programme (UNEP) - SBCI, (2016). http://www.unep.org/sbci/AboutSBCI/Background.asp (accessed February 7, 2017).

[2] Rockwool International, Climate change and energy consumption _ ROCKWOOL International A_S, (2012). http://www.rockwool.com/sustainable+buildings/environment/climate+change+and+energy+consumption? (accessed February 7, 2017).

[3] Rockwool International, Rockwool factsheet. The way towards Nearly Zero Energy Buildings in EU, (2012) 1–8.

[4] EU, Directive 2010/31/EU of the European Parliament and of the Council of 19 May 2010 on the energy performance of buildings (recast), Off. J. Eur. Union. (2010) 13–35. doi:doi:10.3000/17252555.L_2010.153.eng.

[5] A. Lymath, What is a U-value? Heat loss, thermal mass and online calculators explained, 2015. https://www.thenbs.com/knowledge/what-is-a-u-value-heat-loss-thermal-mass-and-online-calculators-explained (accessed February 9, 2017).

[6] M. Gilles, T.D. Jensen, Rockwool International, SRI roadshow Paris, (2011) 1–54. http://www.rockwool.com/files/COM2011/Investor/Presentations/2011/20110610_Paris-SRI-Roadshow_BAML.pdf.

[7] C. Calbraith, The European Market for Thermal Insulation Products, (2015) 5–7.

[8] J.P. Hidalgo-Medina, Performance-based methodology for the fire safe design of insulation materials in energy efficient buildings, The Univeristy of Edinburgh, 2015.

[9] Netzsch, Thermal Insulation Materials - Material Characterization, Phase Changes, Thermal Conductivity, (n.d.) 1–24.

[10] EWI Store, Mineral Wool Insulation vs Expanded Polystyrene, (2015). https://ewistore.co.uk/mineral-wool-insulation-vs-expanded-polysteryne/ (accessed April 22, 2017).

[11] Shree Ram Engineering, Glass Wool Exporter from Ahmedabad, (n.d.). http://www.shreeramengineering.net/glass-wool.html (accessed April 27, 2017).

[12] Paroc, Thermal insulation/stone wool, (n.d.). http://www.archiexpo.com/prod/paroc/product-9579-283531.html (accessed April 27, 2017).

[13] Foam Factory Inc, Expanded Polystyrene Foam: Its Uses, Qualities and Manufacturing Process, (2011). http://www.foambymail.com/blog/expanded-polystyrene-foam-its-uses-qualities-and-manufacturing-process/ (accessed February 13, 2017).

[14] KIMMU, Extruded polystyrene foam, (n.d.). https://en.wikipedia.org/wiki/Polystyrene#Extruded_polystyrene_foam (accessed April 27, 2017).

[15] Global Sources, Phenolic Foam Board for External Wall Insulation, Cold and Heat-resistant, (n.d.). http://www.globalsources.com/si/AS/Adash-New/6008844149693/pdtl/Phenolic-Foam-Board/1047802655.htm (accessed April 27, 2017).

[16] Archi EXPO, Thermal-acoustic insulation/polyisocyanurate (PIR) foam, (n.d.). http://www.archiexpo.com/prod/ediltec/product-103544-1161623.html (accessed April 27, 2017).

[17] Spray Foam Solutions, Waterproofing Solutions with Spray Ployurethane Foam - SPF, (n.d.). http://www.sprayfoamsolutions.co.za/ (accessed April 27, 2017).

[18] J.P. Hidalgo, S. Welch, J.L. Torero, Performance criteria for the fire safe use of thermal insulation in buildings, Constr. Build. Mater. 100 (2015) 285–297. doi:10.1016/j.conbuildmat.2015.10.014.

[19] B. Karlsson, J.G. Quintiere, A Qualitative Description of Enclosure Fires, in: Enclos. Fire Dyn., CRC Press LLC, 2000.

[20] M.G. Davies, The thermal response of an enclosure to periodic excitation: The CIBSE approach, Build. Environ. 29 (1994) 217–235. doi:10.1016/0360-1323(94)90072-8.

[21] D. Drysdale, Fundamentals of the Fire Behviour of Cellular Polymers, in: Fire Cell. Polym., 1986: pp. 61–75.

[22] J.P. Hidalgo, S. Welch, J.L. Torero, Design Tool for the Definition of Thermal Barriers for Combustible Insulation Materials, Proc. 2nd Eur. Symp. Fire Saf. Sci. (2015).

[23] D. Drysdale, Heat Transfer, in: An Introd. to Fire Dyn., 2011: pp. 35–82. doi:10.1002/9781119975465.ch2.

[24] L. Cody, Fire safety considerations for a green and sustainable future, (2011).

[25] EMBUILD, Sandwich Panels /Insulated Panels, (n.d.). http://em-build.com/cladding/purockwooleps/ (accessed April 12, 2017).

[26] Structural Insulated Panel Association, What are SIPs?, (2017). http://www.sips.org/about/what-are-sips (accessed February 20, 2017).

[27] Korwall Industries, Introduction to SIPs, (n.d.). http://korwall.com/website/introduction-to-sips (accessed February 20, 2017).

[28] Covestro AG, Metal-faced Sndwich Panels, (2016). http://www.polyurethanes.covestro.com/en/Applications/Construction/Metal-faced-Sandwich-Panels (accessed February 20, 2017).

[29] Weber, External Insulation Systems, (2017). https://www.sodamco-weber.com/facade-thermal-insulation/products/etics-adhesives-embedding-mortars/webertherm-om.html (accessed April 21, 2017).

[30] EWI Pro Insulation Ltd, What are external thermal insulation composite systems (ETICS)with rendering?, (2016). http://ewipro.com/what-are-external-thermal-insulation-composite-systems-etics-with-rendering/ (accessed February 20, 2017).

[31] Weber, Façade & Thermal Insulation, (2017). https://www.sodamco-weber.com/facade-thermal-insulation.html (accessed April 12, 2017).

[32] Carryduff Designs Architectural Services, Garage conversions, (n.d.). http://www.carryduffdesigns.co.uk/contents/en-us/garage-conversions.html (accessed February 20, 2017).

[33] University of the West of England, Evolution of Building Elements, Univ. West Engl. (2009). http://fet.uwe.ac.uk/conweb/house_ages/elements/print.htm (accessed April 12, 2017).

[34] D. Drysdale, The Pre-Flashover Compartment Fire, in: An Introd. to Fire Dyn., 2011: pp. 349–386. doi:10.1002/9781119975465.ch9.

[35] BS EN 13501-1 Fire Classification of construction products and building elements. Part I: classification using data from rection to fire tests, (2009).

[36] BS EN 1363-1 Fire resistance tests. Part I: general requirements, (2012).

[37] J.P. Hidalgo, J.L. Torero, S. Welch, Experimental Characterisation of the Fire Behaviour of Thermal Insulation Materials for a Performance-Based Design Methodology, Fire Technol. (2016) 1–32. doi:10.1007/s10694-016-0625-z.

[38] R.T. Long, J.L. Torero, J.G. Quintiere, A.C. Fernandez-Pello, Scale and transport considerations on piloted ignition of PMMA, Fire Saf. Sci. (2000) 567–578. doi:10.3801/IAFSS.FSS.6-567.

[39] J.P. Hidalgo, N. Gerasimov, R.M. Hadden, J.L. Torero, S. Welch, Methodology for estimating pyrolysis rates of charring insulation materials using experimental temperature measurements, J. Build. Eng. 8 (2016) 249–259. doi:10.1016/j.jobe.2016.09.007.

[40] Reax Engineering, Gpyro - Generalized Pyrolysis Model for Combustible Solids, (2017). http://reaxengineering.com/trac/gpyro (accessed April 24, 2017).

[41] J.P. Hidalgo, P. Pironi, R.M. Hadden, S. Welch, A framework for evaluating the thermal behaviour of carbon fibre composite materials, Eur. Symp. Fire Saf. Sci. (2015) 195–200.

[42] M.S. Van Dusen, J.L. Finck, Heat transfer through building walls, Bur. Stand. J. Res. 6 (1931) 493. doi:10.6028/jres.006.033.

[43] M. Davies, Building Heat Transfer, John Wiley & Sons, Ltd, 2004.

[44] G.M. Soret, J. Tonino, J.L. Torero, M. Aitchison, Towards optimizing thermal performance of prefabricated houses in Australian climates, (n.d.).

[45] S. V. Szokolay, Heat: the thermal environment, in: Introd. to Archit. Sci. - Basis Sustain. Des., Second Edi, Elsevier Ltd, 2008: pp. 1–93.

[46] G. Proulx, D. Ph, N.R. Cavan, Egress Times From Single Family Houses, (2006). http://www.cfaa.ca/Files/flash/CODES/LIFE SAFETY SYSTEM RESEARCH/egress times from houses rr209.pdf.

[47] HM Government, Approved Document L1A - Conservation of fuel and power, UK Build. Regul. L1A (2013) 1–48.

[48] HM Government, Approved Document L2A - Conservation of fuel and power, Conserv. Fuel Power. L2A (2013) 1–66. http://www.planningportal.gov.uk/uploads/br/BR_PDF_ADL2A_2010.pdf.

[49] K. Butcher, Environmental Design -CIBSE Guide A, 2007.

[50] B. Anderson, Conventions for U-value calculations, Bre 4432006. (2006) 2 to 3.

[51] Magnesium Oxide Board Corporation, MgO Corp Standard Production Sheet Sizes, (2011).

[52] Prasiddha, Standard Brick Size, (n.d.). http://www.civileblog.com/standard-brick-size/ (accessed March 29, 2017).

[53] Belden, Brick Dimensions Guide, (n.d.). http://www.beldenbrick.com/brick-dimensions-guide.asp (accessed March 29, 2017).

[54] Jewson, Standard Plasterboard, (n.d.). file:///H:/Documents/references/Standard Plasterboard - Page 3 _ Plasterboard _ Jewson.htm (accessed March 29, 2017).

[55] Gyprock, Residential Installation Guide - Including Wet Area Systems, 2011.

[56] Structural Insulated Panel Association, SIP R-Values (Calculated R-Values), (n.d.). file:///H:/Documents/references/SIP R-Values (Calculated R-Values).htm (accessed March 29, 2017).

[57] Magnesium Oxide Board Corporation, Magnesium Oxide Board Corporation Sheeting attributes comparison, (n.d.) 2–3. http://mgoboard.com.au/wp-content/uploads/2011/11/Magnesium-Oxide-Board-Comparison-Chart.pdf.

[58] The Engineering Toolbox, Thermal Conductivity, (2006). http://www.engineering.com/Library/ArticlesPage/tabid/85/ArticleID/152/categoryId/11/Thermal-Conductivity.aspx (accessed March 29, 2017).

[59] Knauf Plasterboard, Building with Plasterboard, (2014) 6–29.

[60] J.P. Hidalgo, C. Maluk, A. Cowlard, C. Abecassis-Empis, M. Krajcovic, J.L. Torero, A Thin Skin Calorimeter (TSC) for quantifying irradiation during large-scale fire testing, Int. J. Therm. Sci. 112 (2016) 383–394. doi:10.1016/j.ijthermalsci.2016.10.013.

[61] BS EN 13823 Reaction to fire tests for building products. Building products excluding floorings exposed to the thermal attack by a single burning item, (2010).

[62] J. Zhang, M. Delichatsios, M. Colobert, J. Hereid, M. Hagen, D. Bakirtzis, Experimental and numerical investigations of heat impact and flame heights from fires in SBI tests, Fire Saf. Sci. (2008) 205–216. doi:10.3801/IAFSS.FSS.9-205.

[63] A. Jowsey, Fire imposed heat fluxes for structural analysis, The Univeristy of Edinburgh, 2006.

[64] T. Lennon, D. Moore, The natural fire safety concept - Full-scale tests at Cardington, Fire Saf. J. 38 (2003) 623–643. doi:10.1016/S0379-7112(03)00028-6.

[65] C. Gorska, An Experimental Study of Medium-scale Ccompartment Fire Tests with Exopsed Cross Laminated Timber, 2nd International Fire Safety Symposium. (2017).

[66] J.L.T. G.M. Soret, D. Lázaro, J. Carrascal, D. Alvear, M. Aitchison, Thermal characerization of building assemblies by means of transient data assimilation, (2017).

[67] IGI Global, What is Non-Dominated Solution, (n.d.). http://www.igi-global.com/dictionary/non-dominated-solution/20437 (accessed April 22, 2017).

[68] J.P. Hidalgo, S. Welch, Fire Performance of Plasterboard-Insulation ASseemblies Consisting of Closed-Cell Charring Insulation Mmaterials, (n.d.).

[69] Europerfil, Facade sandwich panel /steel facing, (n.d.).

http://www.archiexpo.com/prod/europerfil/product-50760-729606.html (accessed April 28, 2017).

[70] The Engineering Toolbox, Metals and Alloys - Densities, (2016). http://www.engineeringtoolbox.com/metal-alloys-densities-d_50.html (accessed April 23, 2017).

[71] Physics Resources Database, Thermal Properties - Specific heat capacities, (n.d.). http://www.physics.usyd.edu.au/teach_res/db/d0005c.htm (accessed April 23, 2017).

[72] B.B. Mikic, W.M. Rohsenow, Thermal contact resistance, (1966) 2–91. doi:10.1615/AtoZ.t.thermal_contact_resistance.

[73] HM Government, The Building Regulations 2000 Approved Document B - Fire Safety, (2010).

[74] SFPE, SFPE Handbook of Fire Protection Eng, 2015. doi:10.1080/10543400701199486.

[75] Australian Building Codes Board, Climate Zone Map Australia Wide, (n.d.). http://www.abcb.gov.au/Resources/Tools-Calculators/Climate-Zone-Map-Australia-Wide (accessed April 11, 2017).

Appendix A

Calculation of the required safe egress time

According to Table 2 of Approved Document B, the maximum travel distance for evacuation when only one direction is available in an office or assembly room is 18 m. Figure 50 shows a hypothetical configuration of a room with only one door and a maximum travel distance of 18 m. The area of the room is 324 m².
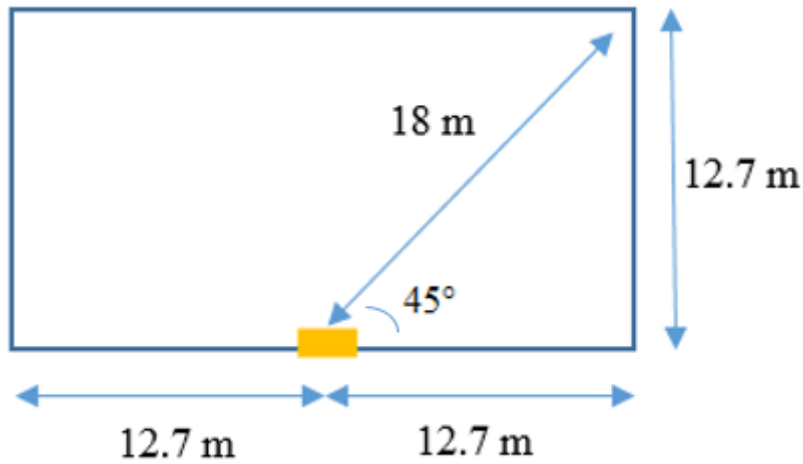

Figure 50: Room configuration

The maximum capacity that a room with only one exit can have is 60 people [73]. This means that the density is:

$$D = \frac{60}{324} = 0.19 \text{ person/m}^2$$

With this density, the specific flow through a doorway can be found in Figure 51 as 0.2 persons/s/m effective width.
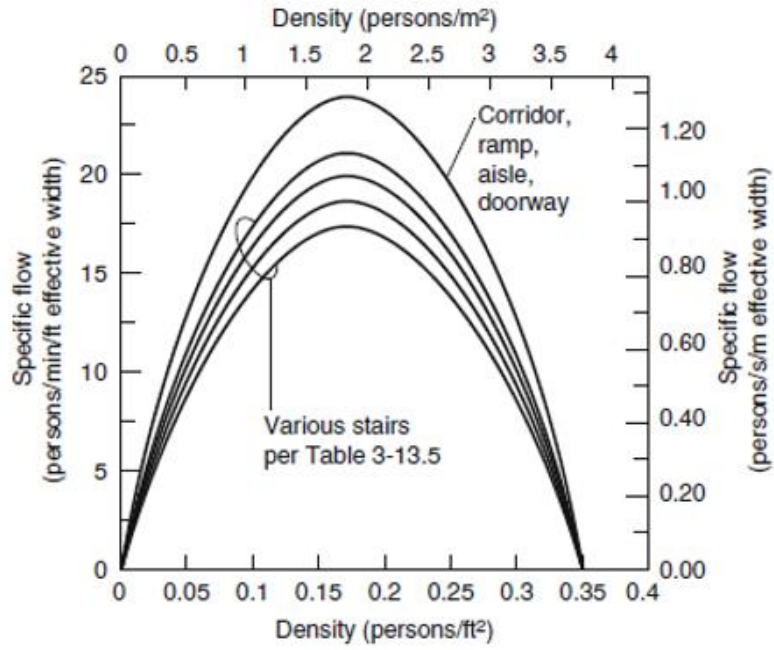
Figure 51: Specific flow as a function of population density [74]

From Table 4 of Approved Document B the minimum width of the doorway can be found to be 750 mm. With this information it is possible to calculate the required time for the 60 occupants to evacuate the room:

$$t = \frac{60}{0.75 \cdot 0.2} = 400 \text{ s}$$

Appendix B

Australian climate zones

The Australian climate zones are [75]:

- zone 1: high humidity summer, warm winter;
- zone 2: warm humid summer, mild winter;
- zone 3: hot dry summer, warm winter;
- zone 4: hot dry summer, cool winter;
- zone 5: warm temperate;
- zone 6: mild temperate;
- zone 7: cool temperate;
- zone 8: alpine.

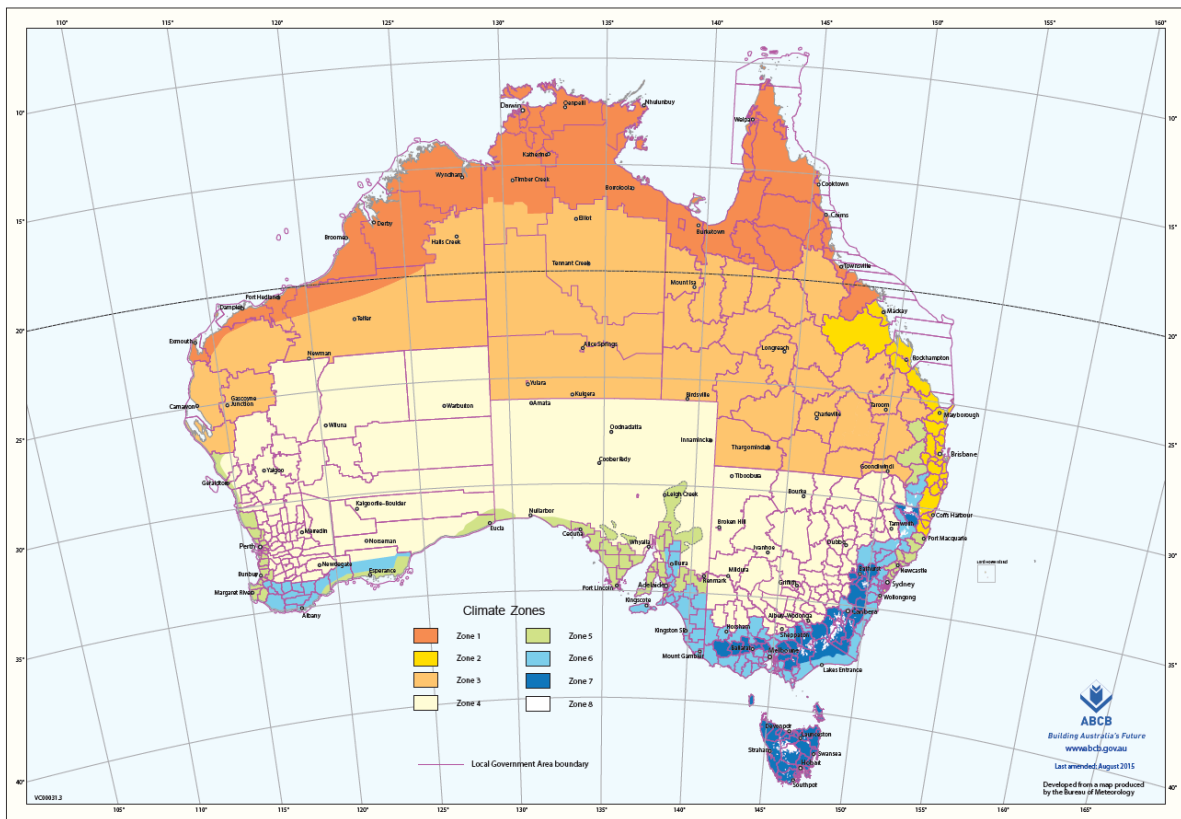Figure 52 shows the 8 different Australian climate zones.

Figure 52: Australian climate zones [75]

Appendix C

Placement of thermocouples

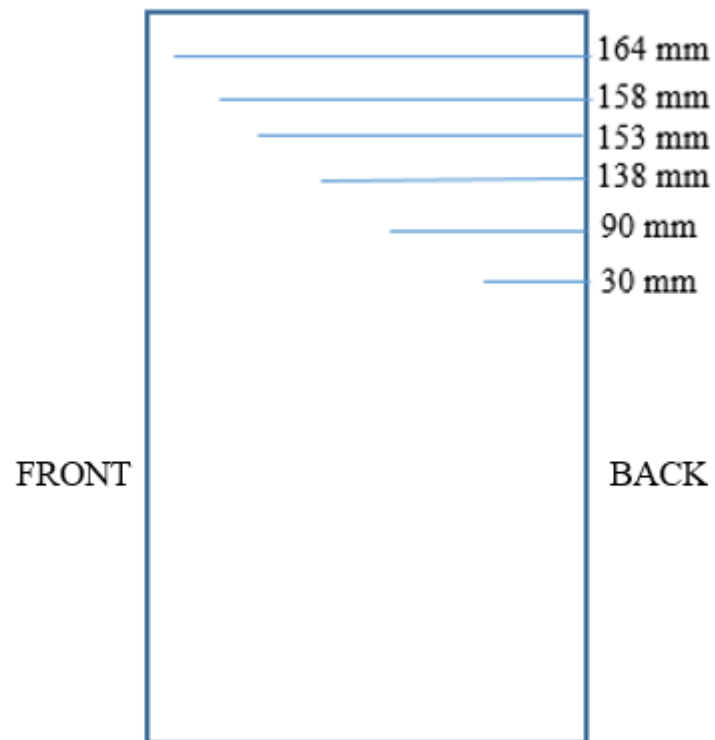Figure 53 shows an example of how the thermocouples were placed during the test.

Figure 53: Example of placement of thermocouples from the back of the sample